Chemical Engineering Journal 338 (2018) 27–45

Contents lists available at ScienceDirect

Chemical Engineering Journal

journal homepage: www.elsevier.com/locate/cej

Review

Two-dimensional MXenes for energy storage

Shuijing Sun[a,b], Chan Liao[a,b], Ahmed M. Hafez[c], Hongli Zhu[c,*], Songping Wu[a,b,*]

[a] School of Chemistry and Chemical Engineering, South China University of Technology, Guangzhou 510641, China
[b] Guangdong Key Laboratory of Fuel Cell Technology, Guangzhou 510641, China
[c] Department of Mechanical and Industrial Engineering, Northeastern University, Boston, MA 02115, United States

HIGHLIGHTS

- This article reviewed the newest progress on electrochemical performance and mechanism of MXenes.
- The relation between electrochemical performance and structure for MXene has been deeply explored.
- The possible directions of development for MXene were also pointed out for energy applications.

GRAPHICAL ABSTRACT

This is a timely and powerful report about present application and future advancement of MXenes in energy storage devices.

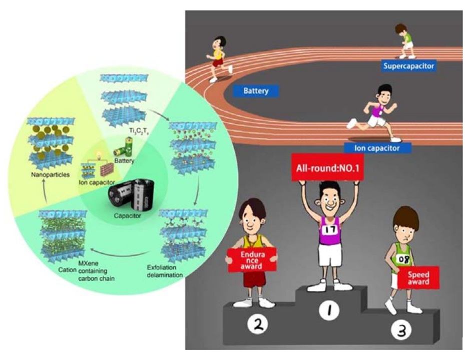

ARTICLE INFO

Keywords:
Two-dimensional MXenes
Energy storage
Review

ABSTRACT

A growing family of MXenes, *i.e.*, layered transition metal carbides and/or nitrides, has been becoming an important candidate of electrode material for new-concept energy storage devices due to their unique properties. This article timely and comprehensively reviewed state-of-the-art progress on electrochemical performance and mechanism of MXenes and their hybrids containing small molecules, polymers or oxides when utilized as crucial materials in energy storage devices, including ion batteries, supercapacitors, and ion capacitors as well as hydrogen storage. The relation between electrochemical performance and structure has been deeply explored in the aims of revealing the influence of logical combinations of chemical/physical properties, microstructure, steric configuration, and material compositions on the electrochemical performance of corresponding electrodes. The possible directions of development for MXene were also pointed out for further researches and potential applications.

1. Introduction

Sustainable development has become the consensus of people all over the world. With the emergence of huge demand for heavy-duty energy storage systems such as electric vehicles, [1] off-grid electricity, [2] and stationary battery systems, [3] high-performance energy storage devices are highly desirable for large power applications. Despite the great achievements, energy storage devices [4–6], such as Li-ion batteries or supercapacitors [7,8] widely used in the present stage, still face two long-term fundamental challenges: (1) It is extremely difficult to simultaneously achieve high energy density and high power density for special device; (2) Limited resources and high cost for recent

* Corresponding authors at: School of Chemistry and Chemical Engineering, South China University of Technology, Guangzhou 510641, China (S. Wu).
E-mail address: chwsp@scut.edu.cn (S. Wu).

https://doi.org/10.1016/j.cej.2017.12.155
Received 27 October 2017; Received in revised form 30 December 2017; Accepted 30 December 2017
Available online 31 December 2017
1385-8947/

rechargeable devices need to be noted. Therefore, development of the new-concept materials with remarkable performance is of most importance and urgency.

Two-dimensional (2D) materials [9] have attracted increasing attention due to their remarkable physical/chemical properties as compared with their bulk counterparts. As a frequently-discussed 2D material, graphene has been regarded as a potential candidate in a wide range of applications [10–12]. Other 2D materials as graphene analogues are imaginably expected to possess extensive chances in next generation energy devices. Layered materials are generally considered to have similar structure as graphene, with planar topology and ultra-thin thickness. Typical graphene-like materials for energy storage include transition metal dichalcogenides (TMDs) [13], transition metal oxides (TMOs) [14]/hydroxides (TMHs), metal sulfides, phosphorenes, MXenes, silicences, etc. [15]. Among them, MXene family, as a type of promising energy storage material, draw our much interest owing to their unique features such as ultra-large interlayer spacing, obvious security capability, environmental benignity and excellent biocompatibility [16,17] (except for some Mxenes, such as $(V_{0.5}Cr_{0.5})_3C_2$ etc). More importantly, these electrodes can not only store relatively large amounts of charge per unit volume or mass, but also discharge at rates that are quite rapid indeed [18]. As to MXene, many excellent far-sighted researchers, such as Prof. Gogosti and coworkers, Prof. Ghidiu and his coworkers and so on, have done a lot of original works. Actually, the review was based on their fruitful researches including simulations and experiments to a considerable degree.

We note that there are several recent reviews on MXenes for energy storage and conversion [19–22]. We concisely analyze those published references to differentiate them with our article. The review by Lei et al. [19] spent a considerable length to introduce the background knowledge of MXenes, mainly based on references published before 2015. In those references [20–22], quite a few layouts were assigned to MXenes. Very recently, numerous applications of MXenes for energy storage and conversion are reported [23,24]. However, there exists a great difficulty in finding a clearly logical relationship between performance and structure/composites for MXene materials in the above references. As stated above, a timely and critical review that exclusively concentrates on MXenes for applications in energy storage devices is fairly lacking until now, particularly based on the perspective of structure/performance.

Herein, we have provided a timely, comprehensive and crucial review, where we have summarized the state-of-the-art developments on the use of MXenes as electrode materials [25] for energy storage devices, mainly ion batteries, supercapacitors and ion capacitors as well as hydrogen storage. The relation between electrochemical performance and structure has been deeply explored. We have paid close attention to the logical combination of the functional directionality of the chemical/physical properties, structure and material compositions. Of special note is that influence of functional groups, microstructure and steric configuration of MXene-based materials on electrochemical performance of corresponding electrodes should be emphatically discussed. To clear the evolution clue of MXene, the timeline of MXene was given as follows. In 2011, the multilayered MXene ($Ti_3C_2T_x$) was first synthesized by selective etching. In 2012, MXene family appeared because a variety of different MXenes such as Ti_2CT_x, $(Ti, Nb)_2CT_x$ and $(V, Cr)_3C_2T_x$ were also produced. Subsequently, single-layer MXene, small flake, double M MXene and ordered divacancies ($Mo_{1.3}CT_x$) have emerged (Fig. 1a) [26]. The general framework for this article has been also given in schematic diagram in the aims of providing a clear outline of the review for the reader (Fig. 1b). As a typical MXene, $Ti_3C_2T_x$ was adopted to depict the research clue of MXene. According to our understanding, creative synthesis of MXene such as $Ti_3C_2T_x$ was the basestone for further researches (marked as $Ti_3C_2T_x$). The next important work is the exfoliation/delamination of MXene, in which small organic molecule (the first in clockwise direction) and ion with small ion radius such as Li^+ ion radius (the second) were first utilized, subsequently, large molecule with long carbon chain and ion was logically chosen as an intercalator (the third). In abovementioned stages, MXenes were considered as promising materials of batteries or capacitors. Along with people knowing more and more about this exciting material, the nanoparticles were finally designed into the interlayers (the 4th), whereby the new-concept device, *e.g.* ion capacitor, began its magnificent performance.

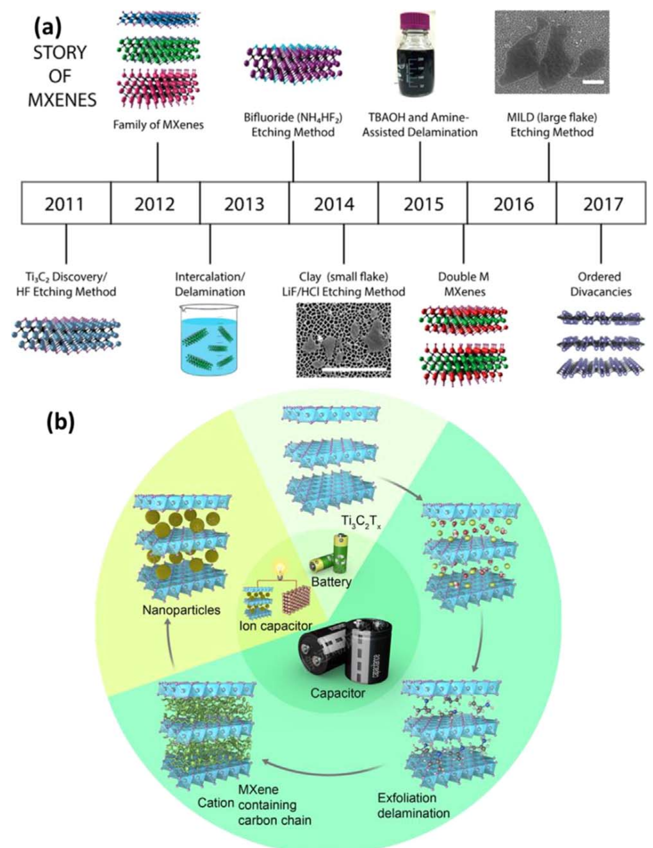

Fig. 1. (a) Timeline of MXene: from Ti_3C_2 discovery to ordered divacancies. Scale bars are 2 μm. Reproduced with permission from Ref. [26] Copyright 2017. American Chemical Society. (b) Schematic diagram on recent research framework of MXenes. As a typical MXene, $Ti_3C_2T_x$ was adopted to depict the research clue of MXene. The research logic and corresponding microstructure of MXene were clockwise exhibited in the outer concentric circles. The devices based on the corresponding materials were clockwise arranged in internal concentric circles.

We hope that ion capacitor can combine the merits of battery and supercapacitor, that is, simultaneously possess high energy density and power density. As a sharp contrast, rechargeable battery has a capability in affording high energy density at the cost of low power density. And, supercapacitor provides high power density with low energy density.

2. Basic information for MXenes

2.1. Family, physical properties and applications

2.1.1. Family

As well-known, MXenes were yielded through exfoliating corresponding three-dimensional MAX phases which have been selectively etched to remove the main-group *sp* elements (denoted A in the MAX), predominantly III A or IV A, and maintained non-corrodible d-block transition metals such as titanium (denoted M in the MAX) and C or N, *e.g.*, X in MAX. It is intriguing to note that the exfoliated layers of MXenes are always terminated with F, OH, and/or O groups during the etching process, whereby these resultant MXene species are generally

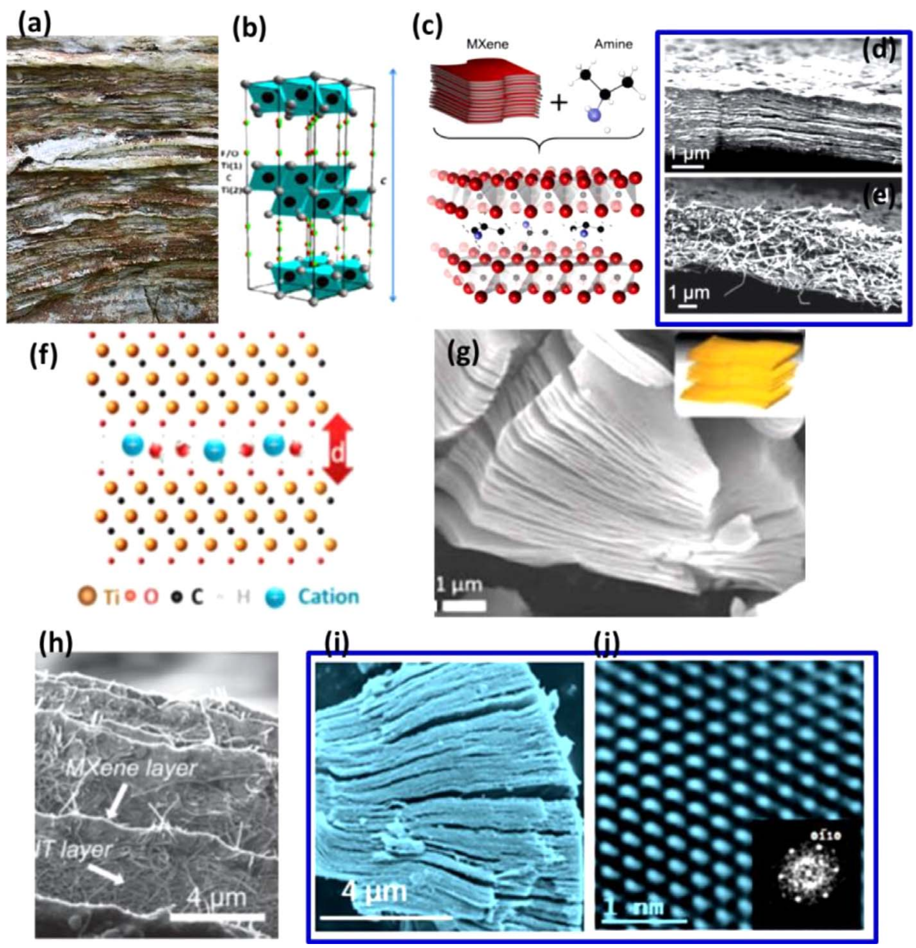

Fig. 2. (a) Typical natural stone with a layered structure. (b) The polyhedral illustration of optimized $Ti_3C_2T_x$ structure. Ti, C, O, and F atoms are in grey, black, red and green colors. Reproduced with permission from Ref. [43] Copyright 2014, American Physical Society. (c) Schematic of Nb_2CT_x delamination process via isopropylamine intercalation. In the schematic, the blue spheres represent nitrogen atoms; red represents niobium; black represents carbon; and white represents hydrogen. (d, e) Cross-sectional SEM images. Reproduced with permission from Ref. [36] Copyright 2015. John Wiley & Sons. f) Schematic illustration of the intercalation of cations between $Ti_3C_2T_x$ layers. (g) Scanning electron micrograph of the $Ti_3C_2T_x$ layered particle. Inset is a schematic of the same. Reproduced with permission from Ref. [44] Copyright 2013. American Association for the Advancement of Science. (h) TEM image of the $Ti_3C_2T_x$/MWCNT papers. Reproduced with permission from Ref. [45] Copyright 2014. John Wiley & Sons. (i) SEM image and (j) lattice resolved HRTEM image (inset shows corresponding FFT pattern) of $Ti_3C_2T_x$ MXene samples annealed in N_2/H_2 atmosphere. Reproduced with permission from Ref. [46] Copyright 2015. American Chemical Society.

assigned as $M_{n+1}X_nT_x$, where T denotes the functional groups (F, OH, and/or O) and x is the corresponding number of terminations.

To date, MXene family includes Ti_3C_2 [27–29], Ti_2C [30,31], V_2C [32], Cr_3C_2 [33], Fe_2C [34], Nb_4C_3 [35], Nb_2C [36], $Mo_{1.33}C$ [37], Mo_2C [38], Hf_3C_2 [39], (V_2C, Cr_2C, and Ta_2C) [40], Cr_2N [41], Ti_4N_3 [42], etc. More MXene materials will be expectedly found in the near future if arduous efforts are persistently paid to the special material system. Typical morphology and structural illustration of MXene and its hybrids have been here depicted so as to provide reference (Fig. 2). Natural stone with a layered structure was utilized to give an example of visualization to better understand the layered structure of MXenes (Fig. 2a). The polyhedral illustration of $Ti_3C_2T_x$ suggested an obvious interlayer structure after removing the A atom in MAX (Fig. 2b) [43]. As a representative polar molecule, isopropylamine was selected as an intercalator to exfoliate/delaminate Nb_2CT_x (Fig. 2c). Cross-sectional SEM images of resultant MXene manifested clearly observable layered structure (Fig. 2d, e) [36]. In another case, intercalation of Li^+, Na^+, Mg^{2+}, K^+, $NH_4{}^+$, and Al^{3+} ions between the 2D $Ti_3C_2T_x$ layers is of great interest in forming enlarged interlayer spacings for $Ti_3C_2T_x$ layered particle (Fig. 2f), as showed in SEM image (Fig. 2g) [44]. Based on exfoliation/delamination of $Ti_3C_2T_x$, flexible, sandwich-like MXene/CNT composite paper electrodes were synthesized through alternating filtration of MXene and CNT dispersions to show a unique 3D structure (Fig. 2h) [45]. More distinctive layered MXenes could be yielded under various atmospheres (Fig. 2i, j) [46].

2.1.2. Physical properties

Because the chemical-physical properties of materials such as structural, mechanical, ion mobility and electronic transport properties are the keystone for corresponding electrodes which were hoped to perform the desired performance, we think that it is of great importance in providing basically physical data for the latest material family.

The conductivity of MXenes has aroused much attention owing to its great influence on electrochemical performance of corresponding electrodes. First-principles calculations based on density functional theory (DFT) has been believed to be a significant method to predict chemical-physical properties of MXenes. DFT showed that Sc-based MXenes such as Sc_2CF_2 [47,48], Sc_2CH_2 and $Sc_2C(OH)_2$ nanotubes [49] and Mo_2CT_x films [50] were semiconductors or semiconductor-like. However, Ti-based MXenes such as atomic (H, Li, or Na) adsorbed $Ti_3C_2T_x$ [51] and Ti_2CO_2 [52] were believed with metallic behavior. The former possessed a density of free carrier of $8 \pm 3 \times 10^{21}$ cm^{-3} and mobility of 0.7 ± 0.2 cm^2/Vs [53], reaching the 9.5×10^4 S/cm of electrical conductance and 54.58 cm^2/V s of hall carrier mobility by the addition of 2.5 wt% of graphene [54]. Conductivity of MXenes such as $Ti_3C_2T_x$ [55] and V_2C [56] were strongly related to Ti vacancy defects

Table 1
Physical Properties of $Ti_3C_2T_x$ and its hybrids.

Composition	Density	Conductivity	Mobility	Tensile strength
$Ti_3C_2T_x$	$8 \pm 3\times10^{21}$ cm^{-3} [53]	2140 S/cm [57]	0.7 ± 0.2 cm^2/Vs [53]	22 ± 2 MPa [59]
$Ti_3C_2T_x$ hybrids	2.7 g cm^{-3} [58]	9.5×10^4 S/cm [54]	54.58 cm^2/Vs [54]	30 ± 3 MPa [59]

for $Ti_3C_2T_x$ MXene and their surface decoration (Table 1, supporting information and Table S1) [57–59]. Molecular dynamics simulations are also used to investigate the structural [60], interfacial [61], and mechanical properties [62] of MXenes. These findings provided a strong understanding of the macroscopic properties of these materials.

2.1.3. Applications

As a group of the state-of-the-art materials, MXenes have been reported to be utilized in many potential areas such as transparent conductors due to a high conductivity of 2140 S/cm [51,57], catalyst supporter of fuel-cell [63], electrochemical biosensors for $Ti_3C_2X_2$ [64], antibacterial membrane [65], magnetic materials for Fe_2C [34], heavy-metal adsorbent [66], ultrasensitive H_2O_2 sensor [67], multicolor cellular imaging [68], spintronic materials [69], optical application [70], superconductors [38], electrocatalysts for Mo_2CT_x [71], and flexible optical/ electronic devices [72].

Obviously, MXenes possess great potentials for a wide range of new concept applications. Here, we want to focus our attention on their most fresh application about energy storage devices due to the inspiring achievements garnered in recent two years [44,73,74]. Before beginning with the detail discussions on those important storage devices, we first hope to introduce the exfoliation/delamination techniques of MXenes, which will provide unique functional groups, microstructure and steric configuration to produce a subtle and profound impact on electrochemical response for corresponding MXene materials.

2.2. Exfoliation/delamination of MXenes

In general, three-dimensional MAX phases are selectively etched to collect corresponding MXenes. There existed two important issues in synthesis of MXenes, *i.e.*, (1) Formation of layered ternary metal carbides, nitrides, or carbonitrides which include selectively erodible elements by HF [75] or LiF/HCl [76], (2) Suitable etching/exfoliation conditions that exerted an important influence on yields and phase conversion of MXenes [77].

We concentrated our concerns on the latter. Recently, structure-stability relationship for 8 MXene alloy systems by high-throughput computations has been discussed, indicating the possibilities of formation of highly ordered MXenes [78]. As-synthesized Ti_3C_2 could be further ultrasonically exfoliated by intercalation with urea, dimethylsulfoxide, ammonia [74], or potassium cations [79]. A universal intercalant of isopropylamine was afterward reported by Gogotsi [36], with which Nb_2CT_x MXenes were allowed to be delaminated by mild sonication in water. Very recently, a work showed that, in the presence of phosphonic acid calix[n]arene (PCXn) in water, ultrasonication of MXene resulted in delaminated MXene with controllable/changeable morphology [80].

The differences between multilayer MXene and delaminated MXene were depicted in Fig. 3 [24]. Herein, we could find that both of multilayer MXene and delaminated MXene owned several remarkable features of interest. (1) MXene possessed an obvious micro-sized hard layered structure because of the ceramic nature, (2) two-dimensional MXene is with a ultralarge layer spacing (~1 nm) of (0 0 2) crystal plane, greater than that of graphite layer (0.337 nm). More importantly, layer spacing could be expanded to some extent, (3) there exist a lot of groups such as O, OH or F group on the surface/interface of MXene, (4) M elements in MXene, such as Ti in $Ti_3C_2T_x$, are fairly active [81]. Those novel features of MXene could bring great enlightenment and great imagination to researchers.

Here, several samples were given to exhibit the expansion of layer spacing and chemical activity of M elements in MXene. As reviewed by Simon [82], Luo et al. reported the preparation of pillared two-dimensional (2D) Ti_3C_2 MXenes with controllable interlayer spacings between 1 and 2.708 nm via intercalation by ion exchange with Sn (+IV) ions, demonstrating a fine-tuned route by creating pillared structures for MXenes. Notably, MXenes annealed under Ar, N_2, and N_2/H_2 atmosphere retained the initial chemical structure [46], and would be destroyed as exposed under an oxidation atmosphere under high temperature [83]. Recent researches showed that Ti_3C_2 MXenes are thermodynamically metastable with poor oxygen resistance even at ambient conditions due to the exposure of large portion of metal atoms on the surface. Therefore, design of carbon nanoplate on surface of Ti_3C_2 MXenes could retain their survive morphology and texture even experiencing annealing process at high temperature [84].

In brief, gradual technology progress has appeared in MXenes, from single ultrasonic exfoliation to intercalation of nanoparticles between layers. Various spin-off methods produced abundant functional groups and steric configuration, and further gave MXene following unique chemical-physical properties.

2.3. Adsorption sites

As shown in Fig. 4, four adsorption sites existed for the functional groups in the MXene sites: [85] a) The functional groups located on the top of the hollow sites above the metal M ions; b) the functional group located on the top of the hollow sites above the X ions; c) the functional groups attached directly on the top of the transition metal (M) ions; and d) some of the functional groups located on the top of the hollow sites above transition metal (M) ions, with other functional groups located on the hollow sites of X ions. Ashton et al. [86] compared the binding energy of O, OH, and F on 2D MXene surfaces in order to find the thermodynamic stability of these compounds and their dependence on their chemical composition. The results suggested that the surface of all MXenes except M = Sc are fully saturated with oxygen, which confirms that MXene surfaces with full functionalization are thermodynamically more stable.

Theoretical calculations directly relevant to ion storage were also investigated, including electronic transport properties of the oxygen/F/ or OH terminated MXene [87], energy barriers of ion intercalation between the layers [88,89], and Li-MXene chemical bonds [90]. Aforementioned theoretical evaluations have laid a solid foundation stone, guaranteeing further research for engineering purposes.

In brief, exfoliation/delamination techniques of MXenes have been increasingly developed along one direction, *i.e.*, how to enlarge layer spacing and form pillars. DFT conclusions have gathered some valuably theoretical achievements for physical property data such as structural stability and conductivity, which are very important parameters for energy storage applications. In the view of an energy storage application, how to efficiently utilize the enlarged layer spacing to achieve excellent electrochemical performance is next urgent issue needs to be addressed.

3. Energy storage applications

In the review, we will provide a comprehensive report on recent advancements in this MXenes for energy storage. There are several parts have been included in the main text, *i.e.*, energy-storage mechanism, different types of energy storage devices based on MXene materials, and finally, we come to some conclusions on the recent research of MXenes and put forward a perspective for future possible direction. Energy storage mechanism has been specifically highlighted for each specific instance.

3.1. Energy storage mechanism

A point of departure for exploiting the unique properties of MXenes in energy storage and conversion devices is the intercalation and delamination. It is well known that MXenes are generally considered to be terminated with functional groups such as F, OH, and O groups after they have experienced a HF exfoliation process [60]. Therefore, energy storage sites were believed to occur at those active groups between layers and surface/interface.

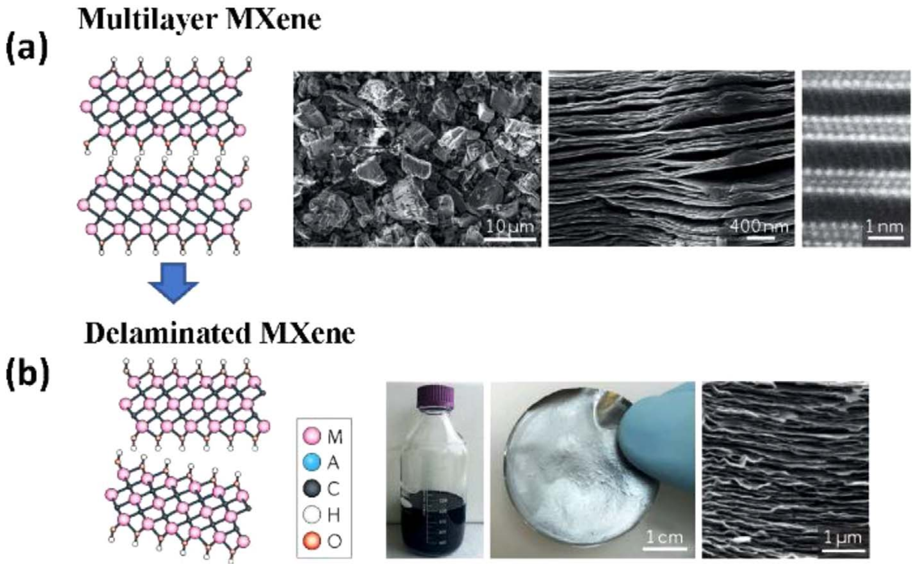

Fig. 3. (a) Illustrations of multilayered MXene. From left to right: schematic diagram of the atomic structure, low magnification and higher magnification SEM images of $Ti_3C_2T_x$ and HR-STEM of Mo_2TiC_2Tx. (b) Illustrations of delaminated MXene. From left to right: schematic diagram of the atomic structure, digital photograph of 400 ml of delaminated $Ti_3C_2T_x$ in water, digital photograph of a Mo_2TiC_2Tx film made by vacuum-assisted filtration, a cross-sectional SEM image of a Mo_2TiC_2Tx film. Reproduced with permission from Ref. [24] Copyright 2017. Macmillan publishers Limited.

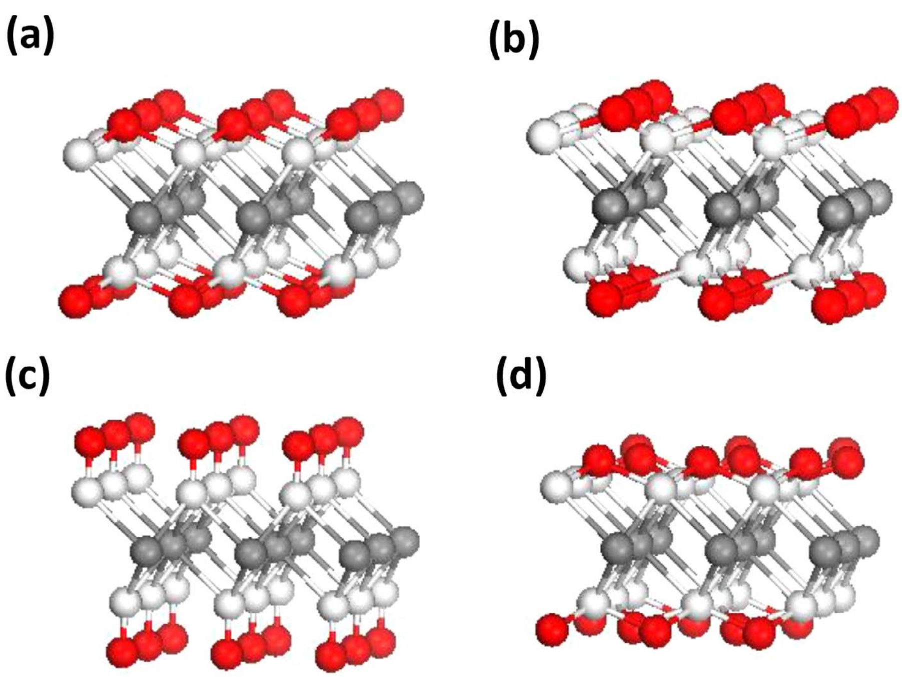

Fig. 4. Adsorption sites for functional groups on 2D Mxene surface. Silver, grey and red represent the M, X ions, and functional groups, respectively. Reproduced with permission from Ref. [85] Copyright 2013. John Wiley & Sons.

3.1.1. Adsorption-desorption

For supercapacitor, charge was predominantly stored in the electrical double-layer on the particle surface or shallow sites [91].

As to rechargeable battery, MXene was generally considered to store energy in the adsorption-desorption manner. DFT theory suggested that lithium was allowed to occupy the most favorable locations, *i.e.*, top sites of the carbon atoms, thereby delivering a theoretical capacity of 320 mAh g^{-1} for Ti_3C_2 [92]. Among functional groups in MXenes, OH group seems to be irreversible for lithium during Li cycling [60]. The subsequently calculated results exhibited that theoretical storage capacity of 413.0 mAh g^{-1} for interlayer-expanded bare Ti_3C_2 MXenes [93]. However, O-terminated MXenes were considered to possess high theoretical capacity [94]. Native point defects, which are proposed to affect the local surface chemistry such as TiO_x, are identified and found to be mobile.

In 2014, Xie et al. reported a complicated mechanism. The O-terminated MXenes may react with ion (such as Na^+ or K^+) to form bare MXenes and metal oxides upon metalization *via* the conversion reactions. Therefore, all the known storage mechanisms, including reversible conversion reactions, insertion/extraction, and plating/stripping, may be found in MXenes [95].

Obviously, more investigations into bare MXenes are very necessary for deeply revealing root cause of their electrochemical performances.

3.1.2. Microstructure and energy-storage groups

3.1.2.1. Microstructure. Introduction of a variety of cations into MXene layers produces large layer spacing in the aims of formation of semipermanent pillars, fine-tunability of MXene conductivity and construction of wide paths for access of different moieties and electrolyte, whereby the more stable, more rapid ion diffusion path could be reconstructed for ion intercalation/de intercalation. A variety of cations such as Li^+, Na^+, K^+, Mg^{2+}, Al^{3+} and $NH_4{}^+$ were allowed to intercalate into MXene layers [44]. Long chain cation of trimethylalkylammonium cations with increasing alkyl chain length were afterwards affirmed to possess the capability of entering interlayer space of MXenes through ion-exchange reaction, enabling the insertion of other alkali and alkaline earth cations [91,96].

Very curiously, the capacitances of $Ti_3C_2T_x$ were modestly influenced by the intercalant chains, indicating that layer spacings/or chain length have not exercised obvious effect over reversible capacity of resultant $Ti_3C_2T_x$.

3.1.2.2. Energy-storage groups. Layered MXenes were intercalated with organic small molecule polar compounds such as hydrazine, N,N-dimethylformamide (DMF) and urea between their layers [74]. Therefore, nitrogen-containing groups were accordingly grafted into MXene [91,96]. Even though N-doped MXene *via* simple solution process do not deliver obviously enhanced electrochemical performance, the nitrogen-doped two-dimensional MXene *via* post-etch annealing $Ti_3C_2T_x$ exhibited drastically improved electrochemical capacitances [97]. The possible reason for the difference is the different bond strength of Ti-N bond in nitrogen-containing MXene, *e.g.*, physical absorption or chemical adsorption. In addition, sulfur-containing MXene also afforded an excellent electrochemical performance, suggesting the emergence of energy-storage groups in doped MXene [81].

Obviously, energy storage mechanism of MXene-based materials is very complicated. We need to broaden our horizons to all possible ways if we want to gather high reversible capacity for rechargeable devices such as Li-ion batteries.

3.1.3. Challenge

As exhibited in recent references, the root cause of energy storage of MXenes appears to be adsorption of sodium/lithium atoms on favorable locations, little to do with the layer spacing. If the postulation is indeed correct, the route to high storage capability of MXenes unexpectedly becomes to be incredibly limited. Zhou et al. [98] studied the intrinsic physical properties of the as-synthesized $Hf_3C_2T_2$ (T = O, F, OH). The electrochemical measurements indicated that the charge storage was due to the intercalation of Li^+ and Na^+ ions rather than a conversion reaction. A further investigation is still needed to find the main cause of MXene electrochemical performance. However, it seems to be difficult to achieve stable Li/Na ion storage performance for MXenes because the electrode materials maybe encounter variously complex physical/chemical environments, which will unavoidably exert critical influences on the adsorption-desorption of sodium/lithium atoms. However, experimental results have explicitly exhibited that MXene indeed possesses stable and reliable electrochemical performance whether they were utilized as battery materials or super capacitor materials. We deduced Ti-containing groups such as TiO_x in MXenes should exert complicated and profound influence over electrochemical performance of corresponding electrodes, where electrochemical mechanism of traditional rechargeable battery should play a subtle role in some ways.

In this case, it is of overwhelming importance in introducing classical Li/Na storage materials into MXene to improve the electrochemical performance of MXene-based materials by means of their highly reversible capacity [99]. Recharge battery and supercapacitor are two representatively complementary electrochemical energy storage devices [100].

In brief, emergence of enhanced layer spacing, conversion of functional groups, formation of intercalated cation and further inorganic materials are the most influential factors for electrochemical performance of MXenes as the electrode of energy storage devices.

3.2. Lithium-ion batteries

Rechargeable lithium-ion batteries have been establishing themselves as prominant roles in portable electronic devices due to a high Li-storage capacity, remarkable cyclability and high reliability. As a commericial anode material, graphite suffers from a low specific capacity of 372 mAh g^{-1} and poor rate capability when utilized in increasing heavy-duty applications. To date, extensive efforts have been made to explore new-concept anode materials to substitute for graphite in LIBs.

3.2.1. Theoretical evaluations

Several references have reported the theoretical Li storage capacity of 320 mAh g^{-1} for Ti_3C_2, gravimetric capacities of 400 mAh g^{-1} for monolayer MXene family (M = Sc, Ti, V, or Cr) [101], nearly comparable with that of graphite. Additionally, excellent high-rate performances for bare Ti_3C_2 MXenes could be reasonably predicted in view of low diffusion barrier for lithium, much lower than that of graphite (0.3 eV). More importantly, the structural transformation of V-type (V_2CO_2, Cr_2CO_2, and Ta_2CO_2) might be reversible during lithiation/delithiation by DFT calculations combined with ab initio molecular dynamic simulations [40]. In another reference [102], adsorption energy of Li for Ti_3C_2 was found to appear little sensitivity to variance in coverage. Chen et al. [103], showed the possibility of applying Ti_3CN and Ti_3CNT_2 (T = O, F, or OH) as anode materials in Li-ion batteries due to their good storage properties, high adsorption activity, and low diffusion barrier.

Above theoretical evaluations have displayed that MXenes are promising anode materials for Li-ion batteries. However, experimental results were extremely needed to meet the practical application requirement.

3.2.2. Bare MXene

Experimental result showed that MXenes possessed a relatively low capacity as anode for Li-ion battery. Here are several examples for reference. Delaminated $Ti_3C_2(OH)_2$ MXene rendered a capacity of 410 mAh g^{-1} at a 1C cycling rate [74]. Free-standing Ti_3C_2 discs under cold pressure afforded an initial reversible areal capacity of 15 mAh cm^{-2}, which decreased to 5.9 mAh cm^{-2} after 50 cycles. Nb_2C delivered the initial reversible capacity of nearly 16 mAh cm^{-2}, and maintained 6.7 mAh cm^{-2} at a rate of 30 mA g^{-1} after 50 cycles [104]. Very recently, layered ternary carbide $Hf_3Al_4C_6$ was etched to form 2D $Hf_3C_2T_z$ MXene *via* introduction of silicon for strengthening the Al (Si) − C bonding and weakening the adhesive energy of the Hf − C (Fig. 5a–e). Such a 2D $Hf_3C_2T_2$ material afforded reversible volumetric capacities of 1567 mAh cm^{-3} (146 mAh g^{-1}) and 504 mAh cm^{-3} (47 mAh g^{-1}) for lithium and sodium ions batteries at a current density of 200 mA g^{-1} after 200 cycles due to the intercalation of Li^+ and Na^+ ions, respectively (Fig. 5f–j) [98]. As to aqueous titanium carbonitride (Ti_3CNT_x) colloidal solution, a discharge capacity of 300 mAh g^{-1} at 0.5 A g^{-1} after 1000 cycles has been gathered [105]. Such a low capacity could be ascribed to surface-controlled kinetics, which could dramatically alter the galvanostatic charge-discharge characteristics, leading to higher overpotentials and lower capacities with increasing mass loading. 2D $Nb_4C_3T_X$ MXene displayed higher capacity than as-produced titanium carbide counterparts [106]. Moreover, the charge/discharge capacity of $Nb_4C_3T_x$ anode increased to 380 mAh g^{-1} (238 mAh cm^{-3}) from 310 mAh g^{-1} (194 mAh cm^{-3}) at a current density of 0.1 A g^{-1} after 100 charge/discharge cycles, and the capacity increased to 320 mAh g^{-1} (200 mAh cm^{-3}) from 116 mAh g^{-1} (73 mAh cm^{-3}) at 1 A g^{-1}.

Solid experimental results strongly suggested that MXenes indeed owned remarkable long-term reversible capacity as anode materials for LIBs, particularly rate performance at large current density. However, the reversible capacity was fairly low for bare MXenes, thereby it is of great difficulty in meeting possible application. In the paper, bare MXenes means the pure Mxenes with normal functional groups rather than “Non-terminated Mxene”

3.2.3. MXene/CNTs

To improve the electrochemical performance, advanced carbon materials such as carbon nanotubes (CNTs) were introduced into the

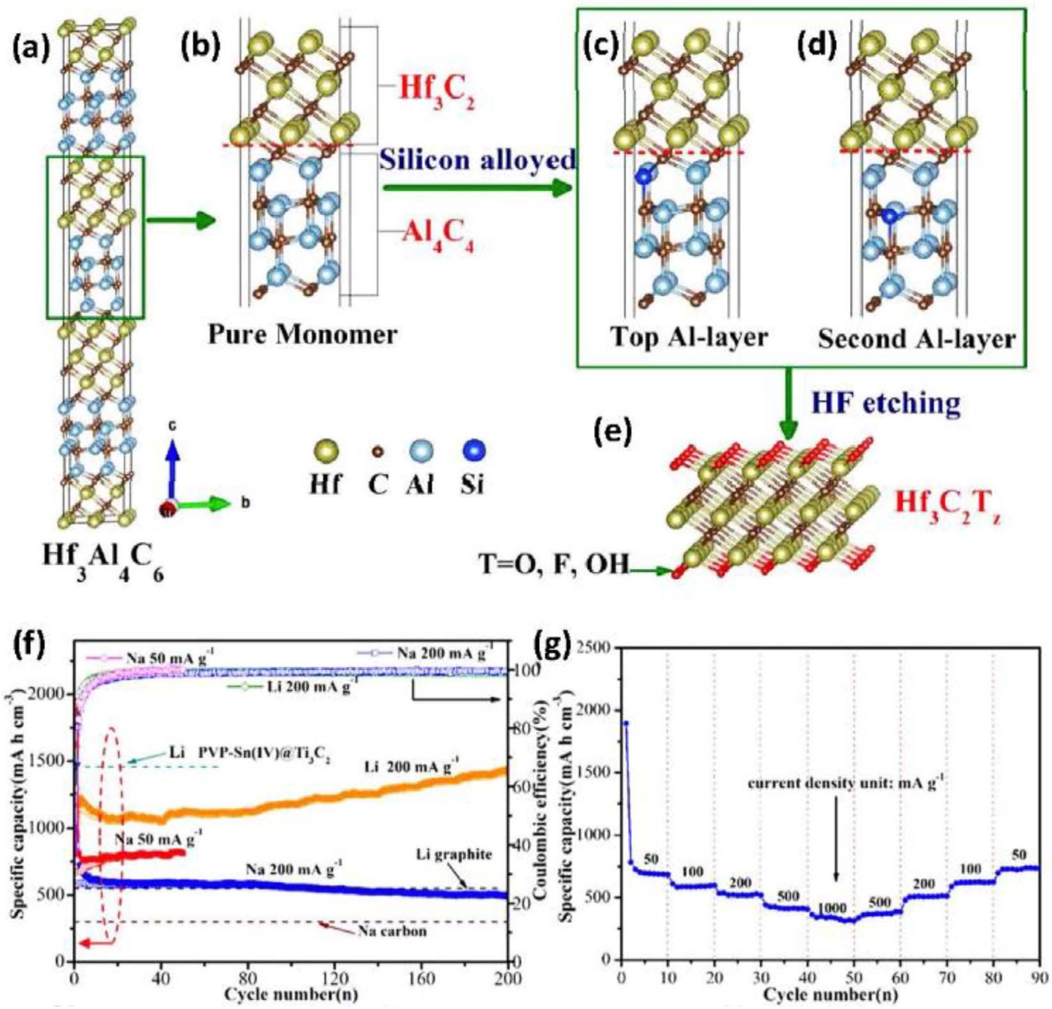

Fig. 5. Schematic diagram showing the fabrication process of the $Hf_3C_2T_z$ MXene: (a) Pure $Hf_3Al_4C_6$ supercell; (b) $Hf_3Al_4C_6$ monomer in its supercell, where the red dashed line denotes the etching interface. (c, d) Silicon alloying in the $Hf_3Al_4C_6$ monomer. Two different replacement positions as (c) in the top Al layer and (d) in the second Al layer are presented. (e) Side view of $Hf_3Al_4C_6$ MXene. (f) Specific charge/discharge capacities, and Coulombic efficiency vs cycle number at different current densities for d-$Hf_3C_2T_z$ MXene in LIBs and SIBs. (g) Rate capability of d-$Hf_3C_2T_z$ MXene for SIBs. Reproduced with permission from Ref. [98] Copyright 2017. American Chemical Society.

MXene to form freestanding, flexible MXene/CNT composite electrodes. Accordingly, specific capacity and resultant rate performance have been enhanced *via* improved ion accessibility. As reported by Gogotsi [36], Nb_2CT_x could be efficiently delaminated in the presence of isopropylamine. Such a freestanding, flexible Nb_2CT_x MXene/CNT composite "paper" electrode afforded an excellent cyclability and Li-storage capacity of ~400 mAh g^{-1} at 0.5C after 100 cycles as an anode material. Notably, in a full battery, Nb_2CT_x anode electrode afforded a capacity of 24 mAh g^{-1} (*i.e.*, volumetric energy density of 50–70 Wh L^{-1}) when $LiFePO_4$ was utilized as cathode materials [107]. Recently, porous free-standing $Ti_3C_2T_x$/CNT films were reported to render significantly improved reversible capacity of 1250 mAh g^{-1} at 0.1C and good rate performance of 330 mAh g^{-1} at 10C [108]. Very recently, Transparent solid-state, asymmetric supercapacitors based on Ti_3C_2Tx/single-walled carbon nanotube (SWCNT) films exhibited high capacitance (1.6 mF cm^{-2}) and energy density (0.05 mu Wh cm^{-2}), and long lifetime (over 20,000 cycles) [109]. Free-standing, flexible Ti_3C_2Tx/CNT for Mg^{2+}/Li^{+} batteries were perceived to deliver a capacity of 100 mAh g^{-1} at 0.1C and 80 mAh g^{-1} at 1C after 500 cycles [110]. Free-standing Mo_2CT_x/8wt%CNTs films delivered a stable reversible capacities of 250 and 76 mAh g^{-1} at 5 A g^{-1} and 10 A g^{-1} for over 1000 cycles, respectively [50].

Several distinctive characteristics have emerged in MXene/CNT hybrids which certainly presented some features of interest.

(1) Sandwich-like assembly of MXenes and CNTs could be formed *via* a simple, alternating filtration method using inexpensive commercial raw materials.
(2) Because the diameter size of CNT is much larger than the interlayer spacings of MXenes, it becomes extremely impossible to enter the MXene interlayers for CNT. Considering to rigid characteristics of MXene ceramic, CNT may twin round MXene particles like a packed package if the MXenes were crushed into ultrafine particles, keeping an integrated structure and enhancing conductivity for MXene/CNT hybrids.
(3) It seems to be easy to make free-standing flexible electrode for MXenes/CNT hybrids. Therefore, significantly high volumetric capacitances and excellent rate performances of MXene/CNT hybrids with artificially designed structure might be gained *via* a cost-effective route.

In brief, even though they possessed considerable rate performance and excellent cycling stability, abovementioned data explicitly demonstrated that MXene materials possessed a comparatively low reversible capacity as compared with other families such as oxides or sulfide. How to promote the electrochemical performance of MXene becomes an actual challenge to be seriously faced before their practical applications will be available in the near future. From this point of view, introduction of oxides into MXene appears to be a logical choice.

3.2.4. MXene/oxides

Recently, there exist two approaches to embed oxides into MXene, and should be discussed as follows: (1) Selectively partial oxidation of MXene [111,112], and (2) Introduction of external metal ion [99,27,113].

3.2.4.1. Selective oxidation of MXene. TiO_2 is a promising candidate as an anode for rechargeable batteries due to its low cost, availability, and environmental friendliness [10]. As mentioned above, Ti_2C could be oxidized to synthesize TiO_2 nanocrystals on their surface·H_2O_2-treated MXene delivered discharge capacities of 389 mAh g^{-1}, 337 mAh g^{-1} and 297 mAh g^{-1} at current densities of 100, 500 and 1000 mA g^{-1} after 50 charge/discharge cycles, respectively, and excellent rate capability of 150 mAh g^{-1} at a high current density of 5 A g^{-1} [111]. $Nb_4C_3T_x$ MXene containing external Nb_2O_5 nanoparticles *via* a one-step partial CO_2 oxidation rendered a capacity of 208 mAh g^{-1} at 50 mA g^{-1} (0.25C), and retained 94% of the specific capacity, with 100% Coulombic efficiency after 400 cycles [112]. A highly porous honeycomb-like structure of NiO nanosheets grown on the surface of $Ti_3C_2T_x$ MXene delivered a high specific capacity of 60.7 mAh g^{-1} at 1 A g^{-1}, with volumetric specific capacity of 92.0 mAh cm^{-3} [83]. Very recently, fully dense Ti_3SiC_2 was electrochemically anodized to produce a thin oxide film based on titania, silica and carbon, rendering specific capacity of 460, 350, and 380 µAh.cm^{-2} after 1st, 2nd, and 140th cycles [114]. Zhao et al. synthesized $Ti_3C_2T_x/Co_3O_4$ or $NiCo_2O_4$ hybrid films using different methods, for instance, alternating filtration method, spray coating and in-situ wet chemistry synthesis. And the spray-coated $Ti_3C_2T_x/NiCo_2O_4$ films showed highest reversible capacities of ≈1330, 650, and 330 mAh g^{-1} at 0.1, 5 and 10C, respectively [115].

In summary, MXene/Oxides have presented following characters: (1) Advantages: Three synergistic effects, *i.e.*, the high conductivity of the interior $Nb_4C_3T_x$ layers, the fast rate response of external Nb_2O_5 nanoparticles, and the electron "bridge" effects of the disordered carbon, have produced deepgoing influences on electrochemical performance of $Nb_4C_3T_x$ MXene [112]. (2) Challenge and prospect: It may be briefly summarized in the following words. Selectively partial oxidation of MXene will *in-situ* form the TiO_2 or Nb_2O_5 nanoparticles in the matrix of Ti/Nb-based MXenes because of their active chemical properties derived from huge defects in crystal structure. It is generally accepted that both TiO_2 [10,11] and Nb_2O_5 [100] possessed excellent rate performances, accompanying with fairly low reversible capacities, very similar with MXenes themselves. Another unavoidable question is that large molar mass of Nb_2O_5 should inevitably lead to a low capacity. Taken together, introduction of TiO_2 or Nb_2O_5 further deteriorated the intrinsic defect of MXene, *i.e.*, low reversible capacity. From another perspective, it may be very difficult to exactly control the reaction conditions of selective oxidation to yield expected production. In exploratory purpose, we considered that *in-situ* formed high-performance oxides such as SnO_2 and Fe_3O_4 in MXene may be hopeful to address its low-capacity problem when used as Li-ion battery materials.

3.2.4.2. Introduction of external metal ion. Tin-based materials were commonly-utilized electrode materials for LIBs owing to their high capacities and environmental benignity [27,99,113]. In 2016, Sn^{4+} ion decorated Ti_3C_2 nanocomposites (PVP-Sn(IV)@ Ti_3C_2, containing 4.93% Sn adsorbed on alk-Ti_3C_2) via a liquid-phase immersion process, afforded a superior reversible volumetric capacity of 1375 mAh cm^{-3} (635 mAh g^{-1}) at 216.5 mA cm^{-3} (100 mA g^{-1}) after 50cycles, higher than that of a graphite electrode (550 mAh cm^{-3}). These nanocomposites retained a stable rate capacity of 504.5 mAh cm^{-3} (233 mAh g^{-1}) even at a high current density of 6495 mA cm^{-3} (3 A g^{-1}) [99]. Recently, Sn(IV)-modified Ti_3C_2 MXene nanocomposites *via* hydrothermal method as anode material for LIBs afforded outstanding initial capacity of 1030.1 mAh g^{-1} at 100 mA g^{-1}, and remained ~360 mAh g^{-1} after 200 cycles [27]. As recently reported by Ahmed et al. [113], HfO_2 coated SnO_2/MXene by atomic layer deposition delivered a specific capacity of 843 mAh g^{-1} at 500 mA g^{-1} at 50th cycle, with a capacity retention of 92%, when used as Li-ion battery anodes cycled in a voltage range of 0.01–3.00 V (vs. Li/Li^+). Wu et al. [84] reported that hierarchical MoS_2/Ti_3C_2-MXene@C nanohybrids *via* assembling carbon coated few-layered MoS_2 nanoplates on carbon-stabilized Ti_3C_2 MXene were with excellent structural stability, electrical properties and strong interfacial coupling, exhibiting exceptional performance of ultra-long cycle life of 3000 cycles with high capacities of ~550 mAh g^{-1} and high capacity retention of 95% (fading rates of 0.0016% per cycle) for Li storage at a very high rate of 20 A g^{-1}. In another interesting reference [116], a new MXene/Ag composite rendered a reversible capacity of 310 mAh g^{-1} at 1C (~320 mA g^{-1}), 260 mAh g^{-1} at 10C, and 150 mAh g^{-1} at 50C, respectively, without capacity decay at 1–50C after 5000 cycles. We want to underscore that the occurrence of Ti(II) to Ti(III) during the cycle process and reduced interface resistance derived from silver may be cause of the long cycle life with high capacity for MXene/Ag composite.

In brief, introduction of external metal ion has exhibited some achievements in improving the reversible capacity of MXene-based materials. However, there existed two issues in recently published references, *i.e.*, limitedly increased capacity [99] and deteriorative cycling stability [27,113], suggesting that further arduous efforts need to be paid to answer those problems.

In this section, the authors summarize the conclusions and put forward some suggestions. As to Li-ion battery application, introduction of oxides could effective improve the reversible capacity of MXene-based materials by means of classical Li-storage mechanism because of the emergence of two electrochemical reactions, *i.e.*, conversion/alloying for oxides and adsorption-desorption for alk-Ti_3C_2 matrix. More efficient and environmentally friendly route should be adopted to intercalate inorganic compounds such as oxides, sulfides and their derivatives with high reversible capacity into interlayers of MXenes, further improve reversible capacity of resultant hybrids. Further efforts need to be performed to achieve a balance between remarkable capacity and high cycling stability. Note that, considering the unique chemical/physical characteristics of MXene, compound precursor and synthesis approach should be carefully chosen to produce corresponding oxides and sulfides perfectly intercalated into interlayers on the premise of keeping integrity of MXene because the chemical stability of MXenes, particular oxidation resistance of titanium element, is obviously inferior to corresponding ceramic materials. We believe that the greatly enhanced reversible capacity will be achieved based on tremendous advancement of advanced battery materials if suitable strategy is deliberately adopted and tactfully accomplished.

Next, we will turn our attention to another type of cost-effective and distinctive rechargeable battery, *i.e.*, sodium ion battery, which will play an important role in energy storage power stations and smart grids in the near future.

3.3. Sodium ion batteries and others

Rechargeable non-lithium-ion (Na^+, K^+ Mg^{2+}, Ca^{2+}, and Al^{3+}) batteries have received much concern as emerging low-cost and high energy-density technologies for large-scale renewable energy storage applications [95,117].

3.3.1. Sodium ion batteries

3.3.1.1. Theoretical evaluations. We first concentrated our interest on the typical sodium ion batteries [11]. As expected, intercalation of K^+ or Na^+ ions expanded the Ti_3C_2 layers perpendicular to the planes by X-ray atomic pair distribution function technique [43]. Reversible sodiation/desodiation between the interlayers was also predicted with NMR integrated with DFT calculation. Further, sodium storage capacities of 413.0, 367.7 mAh g^{-1} and 151.2 mAh g^{-1} for interlayer-

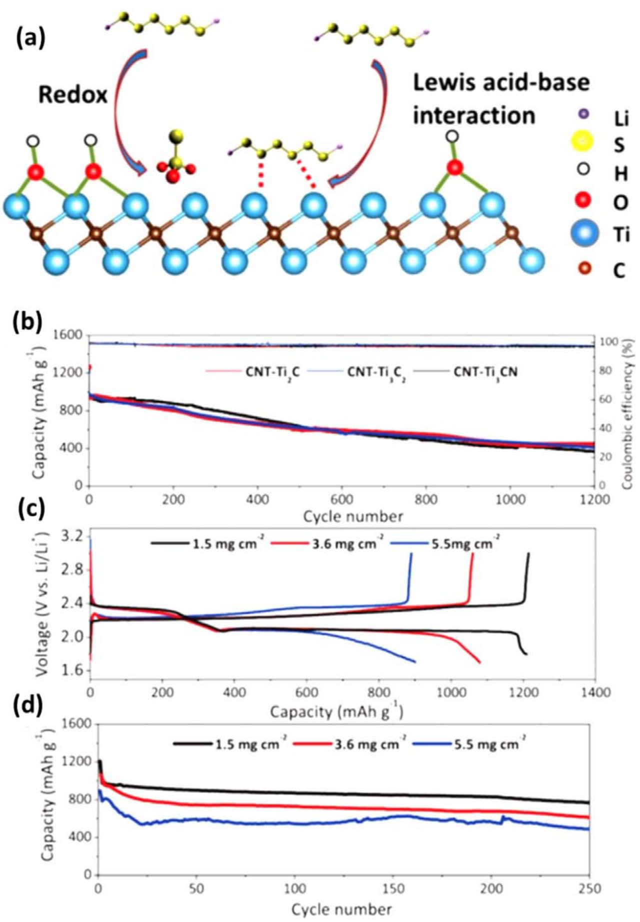

Fig. 6. (a) Schematic demonstrating the two-step interaction between a representative hydroxyldecorated MXene phase and polysulfides. Long-term cycling data for (b) S/CNT-Ti_2C, S/CNT-Ti_3C_2, and S/CNT-Ti_3CN with a sulfur loading of 1.5 mg cm^{-2}, measured at a rate of C/2. (c) Electrochemical performance of S/CNT-Ti_3C_2 electrodes with high sulfur loadings. Reproduced with permission from Ref. [81] Copyright 2017. John Wiley & Sons.

expanded bare and O-functionalized Ti_3C_2 and F-functionalized Ti_3C_2 MXenes have been theoretically calculated [93], respectively, with almost negligible volume changes (−0.5% to +1.6%) during sodiation and desodiation. Based on above theoretical assessment, experimental explorations have been continuously carried out as follows.

3.3.1.2. MXenes and MXene-based hybrids. To date, experimental result of sodium half cells suggested a low reversible capacity for MXene materials. In a literature, Ti_3C_2 delivered a specific capacity of 100 mAh g^{-1} at a current density of 20 mA g^{-1} after 100 cycles [118]. Subsequently, MoS_2-intercalated $Ti_3C_2T_x$ layers *via* a hydrothermal route were reported to render an improved high specific capacity of 250.9 mAh g^{-1} over 100 cycles, and rate performance with a capacity of 162.7 mAh g^{-1} at 1 A g^{-1} [119]. In another half sodium-ion cell [120], freestanding Ti_3C_2 MXene/CNTs porous films delivered a high volumetric capacity of 345 mAh cm^{-3} at 100 mA g^{-1} after 500 cycles (reversible capacity of 175 mAh g^{-1} at 20 mA g^{-1} after 100 cycles). Bak et al. [121], synthesized and studied 2D vanadium carbide MXene V_2CT_x as anode material, exhibiting a reversible capacity of 78 mAh g^{-1} up to 100 cycles at a current density of 20 mA g^{-1}. However, side reactions and electrolyte decomposition contributed to large irreversibility and low Coulombic efficiency. 3D MXenes films, such as Ti_3CT_x, V_2CT_x, Mo_2CT_x, were proved to show enhanced electrochemical performance of the reversible capacity of 295, 310, 290 mAh g^{-1} at 2.5C (1C = 200 mA g^{-1}) after 1000 cycles, better than multilayer MXenes or MXenes hybrids [122]. Very recently, K^+ intercalated Ti_3C_2 MXene nanoribbons exhibited remarkable sodium/potassium storage performance, *e.g.*, reversible capacities of 168 and 136 mA h g^{-1} at 20 mA g^{-1} and 84 and 78 mA h g^{-1} at 200 mA g^{-1} for SIBs and PIBs, respectively [123]. Recently, Sb_2O_3/MXene ($Ti_3C_2T_x$) hybrid materials were firstly fabricated for sodium storage, delivering a rate performance of 295 mA h g^{-1} at 2 A g^{-1}, and an enhanced cycling performance of 472 mAh g^{-1} after 100 cycles at 100 mA g^{-1} [124].

Such a low capacity showed that the investigation into sodium storage mechanism is still in its infancy. At present, the most critical factor is gradual development of research framework including core electrode materials, compatible electrolyte and separator with excellent Na-ion penetration, *etc*.

As to full battery, some fruitful and enlightening attempts have been also carried out to check the potential of practical application. Prototype sodium-ion full cells were also assembled using the as-prepared Ti_3C_2/CNTs anode and $Na_{0.44}MnO_2$ cathode, powering a 2.5 V light-emitting diode (LED) for ~25 min, expending an electrical energy of 0.041 mW h [120]. The first charge/discharge capacities for the full cell were 270 and 286 mAh cm^{-3} based on the volume of the $Ti_3C_2T_x$/CNT-SA electrode, respectively, and retained a volumetric discharge capacity of 242 mAh cm^{-3} after 60 cycles at a current density of 50 mA g^{-1}, with a high Coulombic efficiency (99%). In another full Na ion battery, a capacity of 50 mAh g^{-1} with a maximum cell voltage of 3.5 V has been gained using hard carbon as negative electrode [125].

In summary, low capacity and poor rate capability of anodes are still the bottlenecks for SIBs. More works, including theoretical assessment and experimental progress, should be performed to accumulate more technical data, further gradually tackle those formidable problems in the future.

3.3.2. Other devices (Li-S battery)

Li–S batteries have recently garnered much attention owing to the simple configuration, high capacity and energy density, and environmentally friendly materials of sulfur. As reported in a reference published in 2015 [126], 70 wt% sulfur/Ti_2C composite cathodes showed a specific capacity close to 1200 mAh g^{-1} at a C/5 current rate, accompanying with a capacity retention of 80% over 400 cycles at a C/2 current rate. In another research [127], $Ti_3C_2T_x$ MXene delivered a discharge capacities of 550 mAh g^{-1} at 0.5C and 495 mAh g^{-1} at 1C after 500 cycles. In another reference, TiC@G/S as cathode for Li-S battery without binder, separator and current collector was reported to exhibit a capacity of 670 mAh g^{-1} at a current density of 0.2C (1.17 mAh cm^{-2}) after 100 cycles, with columbic efficiency of over 95% [128].

Carbon/sulfur is a typical cathode for Li-S battery. Zhao and his co-workers proved that multi-layers carbon/sulfur flakes derived from MXenes Ti_2SC showed promising performance as Li-S battery cathode [129]. Roll-to-roll mechanical approach was used to fabricate Lamellar structured flexible Ti_3C_2 MXene (graphene, BN)-lithium film, with relatively low overpotential, exhibited high reversible capacity of 841 mAh g^{-1} after 100 cycles for a lithium-sulfur full cell with Ti_3C_2-Li as anode and sulfur-carbon as cathode [130].

High long-term capacity is highly desirable for Li-S battery. Very recently, interwoven MXene nanosheet/CNT composites were synthesized [81]. The hydroxyl terminal groups on MXene first react with polysulfides to form the thiosulfate groups, followed by the Wackenroder reaction that exposes the Ti atoms (Fig. 6a). Interweaving CNTs between the MXene layers produced a porous, electronically conductive network, where high polysulfide adsorption enabled sulfur hosts with excellent long-term cycling performance, *e.g.*, reversible capacities of ~450 mAh g^{-1} after 1200 cycles at a C/2 rate with capacity retention of ~95% (fading rates of 0.043% per cycle) (Fig. 6b–c) [81]. More importantly, excellent performance could be available even at high loading of 5.5 mg cm^{-2}. In another intriguing work [131], 3D $Ti_3C_2T_x$/rGO/sulfur composites *via* a liquid phase impregnation method delivered high initial capacity of 1144.2 mAh g^{-1} at 0.5 °C and a high level of capacity retention of 878.4 mAh g^{-1} after 300 cycles when applied as a cathode host material for lithium sulfur batteries.

For rechargeable non-Li-ion batteries, a summary has been presented as follows. Even though theoretical predictions have given us a bright prospect for SIB application, experimental results suggested low capacity and poor rate capability of existing anodes. Preliminary researches indicated that introduction of carbon materials such as CNTs could provide an opportunity to develop free-standing electrode, however, low reversible capacity is still the obstacle for future developments.

As to Li-S batteries, ultrastable reversible capacity has been displayed upon long-term cycling. However, it is noteworthy that Ti-OH groups are replaced by sulfur (or S^{2-}) to form Ti-S bonds at elevated temperature during the heat treatment [126], and strong Ti-S bonds has been found to dominate the interactions between Li_2S_m@MXenes [132]. It is very possible that three materials including MXene loading sulfur, sulfide derived from MXene or mixtures of the two coexist in active electrode materials. Therefore, exactly active material compositions might need to be further recognized and clarified with more solid evidences.

3.4. Supercapacitors

Fast ion adsorption process in supercapacitors enables quick storage/delivery of significant amounts of energy, while ion intercalation in battery materials leads to even larger amounts of energy stored, but at substantially lower rates due to diffusional limitations [18]. Clearly, the batteries afford high energy density but low power density and supercapacitors provide high power density with low energy density [100]. Colloidal pseudocapacitor [133,134], as one kind new-type energy storage device, have been reported to make great progress in recent years [135]. The maximum surface area along with nanosized cavities and open channels are the important parameters determining the electrochemical performance of pseudocapacitive electrode materials [136]. Here, we drew our attention to "normal" supercapacitors which adopt inorganic such as KOH [137,138] or H_2SO_4 [139] as electrolyte.

3.4.1. Theoretical evaluations

Intercalation of ions into 2D $Ti_3C_2T_x$ (MXene) has given rise to a very high rate and capacitance. Such a capacitive paradox was considered to be originated from cationic insertion, accompanied by deformation of the MXene particles, that appeared so rapidly so as to resemble 2D ion adsorption at solid-liquid interfaces in the presence of water molecules between the MXene sheets [18]. Subsequently, Ji and coauthors took advantage of first-principles approach to evaluate performance of O-terminated Ti_2C nanosheets, suggesting a simulated capacitance of 291.5 F g^{-1} for integral capacitance and Na-ion capacity of Ti_2CO_2 nanosheets in a potential window from 0 to 2.80 V (versus Na/Na^+). The electrochemical performance could be originated from large intrinsic capacitance and contact adsorbed cations [140]. Still later, an investigation into mechanical properties may be indicative of a strong correlation between the cations content and the out-of-plane elastic modulus for 2D titanium carbide ($Ti_3C_2T_x$) based electrode, identifying the preferential intercalation pathways within a single particle [141]. Obviously, MXene-based materials exhibited huge potential for supercapacitor application which will be corroborated by following experimental results.

3.4.2. $Ti_3C_2T_x$ MXenes

Some efforts have been devoted to $Ti_3C_2T_x$ MXenes including their CNT hybrid films [45], doping [97], electrolyte and devices [142,143]. In 2014, Ghidiu and coworkers reported that a clay-like $Ti_3C_2T_x$ material *via* rolling as supercapacitor electrodes in a H_2SO_4 electrolyte rendered volumetric capacitance of 900 F cm^{-3} or 245F g^{-1} (Fig. 7) [73]. A clay-like paste could be rolled in a roller mill to efficiently form flexible, free-standing films.

3.4.2.1. Group removing/ion intercalation. Remove of terminal groups such as OH^- and F^- and/or intercalation of alkali cations could significantly improve the capacitance of MXene. In 2015, the tunable 2D Ti_2CT_x MXene sample annealed in N_2/H_2 atmosphere achieved an excellent rate performance at current densities ranging from 1 to 40 A g^{-1}, rendering specific capacitance of 51 F g^{-1} at 1 A g^{-1} when used in symmetric two-electrode configuration, with remarkable cycling stability, *i.e.*, retention of 93% after 6000 cycles [46]. In 2017, after K^+ intercalation and terminal groups (OH^-/F^-) removing, MXene sheets exhibited a significant enhancement (~211%) in the gravimetric capacitance (517F g^{-1}@1 A g^{-1}), with ~99% retention over 10,000 cycles [144]. Li-intercalated $Ti_3C_2T_x$ afforded an improved electrochemical capacitive property of 115F g^{-1} at 200 mV s^{-1} [145].

3.4.2.2. Binder-free MXene film. In 2017, the binder-free MXene films also aroused much attention. The binder-free $Ti_3C_2T_x$-based films *via* electrophoretic deposition delivered high capacitance of ~140F g^{-1} in alkaline electrolyte, without capacitance fading after 10,000 cycles [146]. Notably, highly accessible macroporous electrode architectures of $Ti_3C_2T_x$ MXene film delivered an excellent capacitance of 210 F g^{-1} at 10 V s^{-1} rate. In-situ incorporation of the H_2SO_4 electrolyte between MXene layers gave a volumetric capacitance of ~1500 F cm^{-3}, reaching the previously unmatched volumetric performance of RuO_2 [147]. The freestanding MXene/rGO *via* electrostatic assembly displayed a volumetric capacitance of 1040 F cm^{-3} at a scan rate of 2 mV s^{-1}, an impressive rate capability with 61% capacitance retention at 1 V s^{-1} and long cycle life [58].

3.4.2.3. Doping. Doped MXenes were also concerned [148]. Very recently, nitrogen-doped $Ti_3C_2T_x$ by post-etch annealing rendered drastically improved electrochemical capacitances of 192 F g^{-1} in 1 mol L^{-1} H_2SO_4 and 82 F g^{-1} in 1 mol L^{-1} $MgSO_4$ electrolyte for supercapacitors [97]. Yang et al. [149], reported high-capacity for codoped nitrogen and sulfur titanium carbide (NS-Ti_3C_2), which prepared from Ti_3C_2 nanosheets after a simple thiourea-assisted carbonization process. The treated NS-Ti_3C_2 nanosheets exhibited high specific capacitance of 175F g^{-1} at 2 mV s^{-1} in 1 mol L^{-1} Li_2SO_4 electrolyte solution, with a large cyclic stability reached to 90.1% of the initial capacitance after 5000 cycles.

3.4.2.4. Electrolyte. As an important component, electrolyte for $Ti_3C_2T_x$ MXene also attracted much concerns. Recently, there are researches on ionic liquid electrolyte for $Ti_3C_2T_x$ MXene [150,151]. $Ti_3C_2T_x$ MXene ionogel film by vacuum filtration delivered a capacitance of 70F g^{-1} together with a large voltage window of 3 V at a scan rate of 20 mV s^{-1} in neat EMI-TFSI electrolyte, *i.e.*,1-ethyl-3-methylimidazolium bis (trifluoromethylsulfonyl) imide neat ionic liquid electrolyte [151]. Such a performance was ascribed to either electrostatic attraction effect between intercalated TFSI-anions and positively charged $Ti_3C_2T_x$ nanosheets or steric effect caused by de-intercalation of EMI^+ cations through *in-situ* X-ray diffraction investigations [150]. Solid electrolyte is of great interest in providing more safe devices.

3.4.2.5. Microdevice. Logically, microdevices aroused much interest for preliminary practical application. Clay-like Ti_3C_2 MXene microsupercapacitor delivered a capacitance of 25 mF cm^{-2} at 20 mV s^{-1}, affording an energy density of 0.77 μ Wh cm^{-2} at power density of 46.6 mW cm^{-2} [143]. In 2015, the free-standing and highly flexible sandwich-like $Ti_3C_2T_x$/MWCNT papers exhibited significantly high capacitances of 150 F g^{-1} (321 F cm^{-3}) at a scan rate of 2 mV s^{-1}, and around 117 F g^{-1} (250 F cm^{-3}) even at 200 mV s^{-1} [45]. Zhu et al. [152] revealed that l-Ti_3C_2 intercalated with polypyrrole (PPy) could enhance the overall performance in terms of both capacitance and

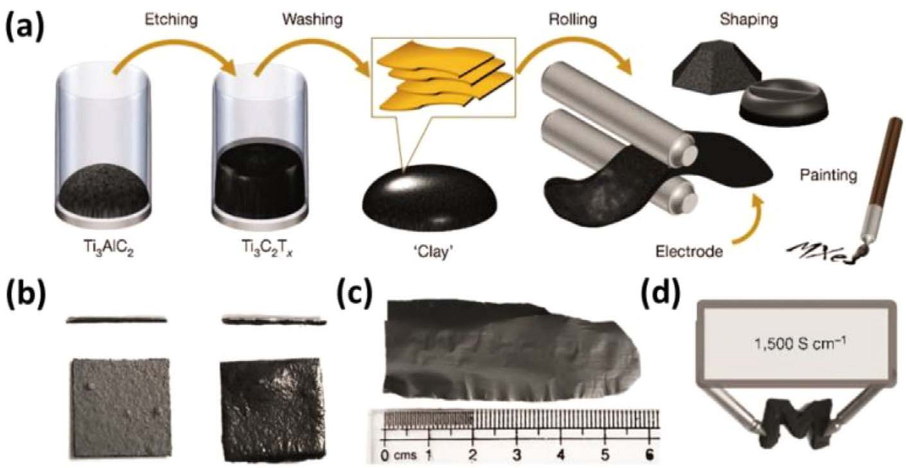

Fig. 7. Schematic of MXene clay synthesis and electrode preparation. (a) MAX phase is etched with mixture of acid and fluoride salt, then washed with water to raise the pH towards ~7. The resultant sediment looks like a clay; and can be rolled to produce flexible, freestanding films, moulded and dried to yield conducting objects of desired shape, or diluted and painted onto a substrate to gather a conductive coating. (b) When dried samples (left, showing cross-section and top view) are hydrated (right) they swell; upon drying, they shrink. (c) Image of a rolled film. (d)"Clay"shaped into the letter M (1 cm) and dried, yielding a conductive solid (labelled with the experimental conductivity of "clay" rolled to 5 mm thickness). The etched material is referred to as $Ti_3C_2T_x$, where the T denotes surface terminations, such as OH, O and F. Reproduced with permission from Ref. [73] Copyright 2014. Macmillan publishers Limited.

stability. The l-Ti_3C_2 plays a role in preventing the stacking of PPy, thus providing a higher electrochemical activity and precise ion migration.

All-MXene (typical $Ti_3C_2T_x$) solid-state interdigital micro-supercapacitors by a solution spray-coating method exhibited a much low contact resistance, high capacitances and good rate-capabilities, *i.e.*, a real capacitance of 27.3 mF cm^{-2} at a scan rate of 20 mV s^{-1} and a volumetric capacitance of 356.8 F cm^{-3} at 0.2 mA cm^{-2}, respectively, with 100% capacitance retention after 10,000 cycles at a scan rate of 50 mV s^{-1} [142]. Very recently, flexible all-solid-state rGO/$Ti_3C_2T_x$ (MXene) film-based supercapacitors has been developed [153], rendering volumetric and gravimetric capacitance of 370 F cm^{-3} and 405 F g^{-1} in 6 mol L^{-1} KOH solution, respectively. At a power density of 0.06 W cm^{-3}, the assembled supercapacitors delivered an energy density of 63 mW h cm^{-3}.

The scalable process has been developed, for example, $Ti_3C_2T_x$ (HCl–LiF etched) clay electrodes with thicknesses of 75 μm showed capacitance of 350 F cm^{-3} (Fig. 8), suggesting that MXenes other than $Ti_3C_2T_x$ also demonstrate much promise for supercapacitors [24].

Extensive researches have been performed in wide fields of supercapacitor including material synthesis, microdevices and electrolyte. To date, electrochemical performances of MXenes are obviously low and needs to be improved to meet high energy application.

3.4.3. MXene/organic compounds

AA cations of $[(CH_3)_3NR]^+$ were chosen as intercalator to collect intercalated MXenes with different alkylammoniums (Fig. 9a) [91], where R is an alkyl chain of variable length. The almost unchanged capacitances at high scan rates indicated that charge was predominantly stored in the electrical double-layer on the particle surface or shallow sites in the interlayer at scan rates of 50 mV s^{-1} and above (Fig. 9b, c). Subsequently, organic compounds with long carbon chain were also adopted to intercalate into MXenes for changing viscosity, conductivity and degree of crystallization of MXene-based hybrides [154], facilitating charge transport in supercapacitor electrodes. Afterwards, polymer was introduced to $Ti_3C_2T_x$ to gather polymer/$Ti_3C_2T_x$ composites. The resultant MXene/PVA-KOH composite film afforded an impressive volumetric capacitance of similar to 530 F cm^{-3} at 2 mV s^{-1} [59]. Further, conductive polymer, *i.e.*, heterocyclic pyrrole molecules, are *in-situ* aligned and polymerized between layers of the 2D $Ti_3C_2T_x$ (MXene) in the absence of an oxidant, giving rise in high volumetric capacitance of 1000 F cm^{-3} at a 100 mV s^{-1} scan rate, with capacitance retention of 92% after 25,000 cycles [155].

In brief, conductive polymer provided the more conductivity and held the layer spacing to facilitate charge transport of MXenes, leading to enhanced electrochemical performance. However, the huge molar mass of conductive polymer is an obvious disadvantage for further improvement of capacitance. Therefore, oxides should be next goal to be chosen for desirable performance.

3.4.4. MXene/oxides

TiO_2-decorated Ti_3C_2 MXene nanosheets *via* hydrolysis followed by heat-treatment rendered high specific capacitance of 143 F g^{-1} at 5 mV s^{-1} and excellent cycling stability, with 92% capacitance retention after 6000 cycles [156]. When 2 μm thick films were tested as electrodes in supercapacitors, capacitance of 2D Mo_2CT_x was up to 700 F cm^{-3} (196F g^{-1}) at 2 mV s^{-1} in a 1 mol L^{-1} sulfuric acid electrolyte, accompanying with high capacity retention for at least 10,000 cycles at 10 A g^{-1} [50]. Recently, nanocrystalline ε-MnO_2 whiskers were formed on MXene nanosheet surfaces (ε-MnO_2/Ti_2CT_x and ε-MnO_2/$Ti_3C_2T_x$) to make nanocomposite electrodes for aqueous pseudocapacitors. The surface area of the composite electrode is nearly increased by nearly 3 times as compared with the pure MXene counterparts. As a result, ε-MnO_2/MXene supercapacitors afforded an excellent cycling stability, with 88% capacitance retention after 10,000 cycles

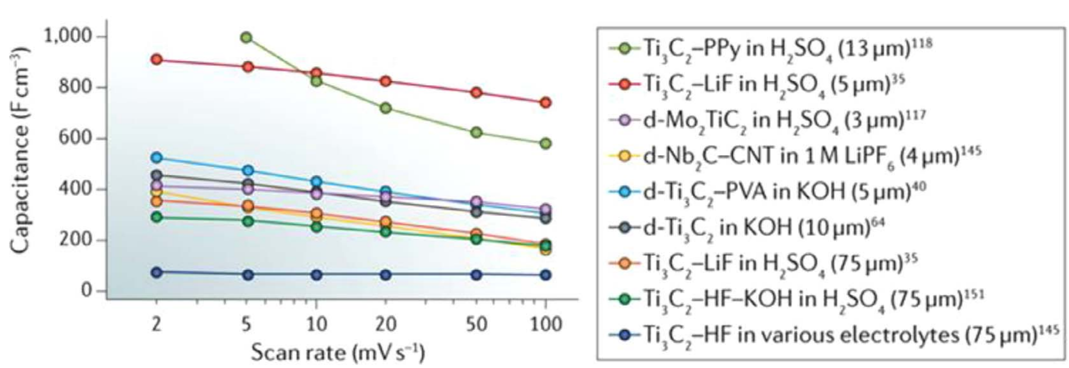

Fig. 8. Comparison of rate performances of MXene electrodes. Reproduced with permission from Ref. [24] Copyright 2017. Macmillan publishers Limited.

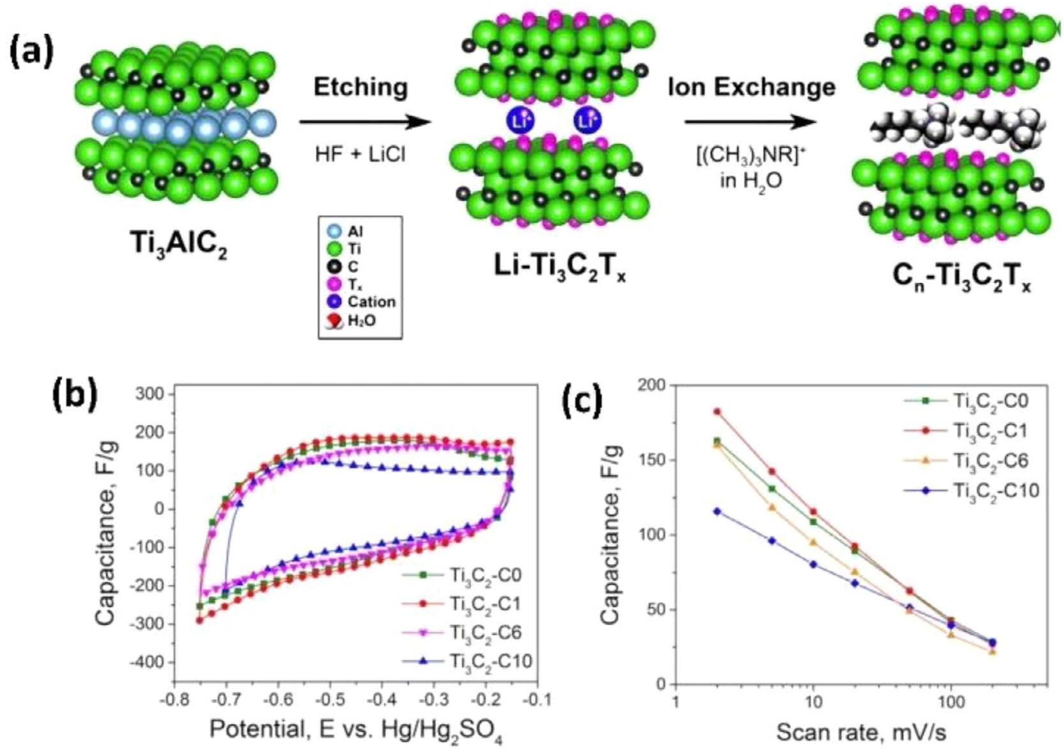

Fig. 9. (a) Schematic of materials produced. First, Ti_3AlC_2 is etched with HF + LiCl to yield Li–Ti_3C_2Tx, which is then ion-exchanged with trimethylalkylammonium chlorides or bromides. The structures in the interlayer of C_n-$Ti_3C_2T_x$ represent alkylammonium cations. (b) cyclic voltammagrams of nonintercalated (C_0) and intercalated C_1, C_6, and C_{10} samples; (c) gravimetric capacitance as a function of scan rate. Reproduced with permission from Ref. [91] Copyright 2017. American Chemical Society.

[157]. In another reference, 2D delaminated Ti_3C_2 nanosheets decorated with MnOx nanoparticles by electrostatic interactions exhibited a volumetric capacitance of 602.0 F cm^{-3} at 2 mV s^{-1} [158].

The brief summary has been given to supercapacitor section. The macroporous electrode architectures of $Ti_3C_2T_x$ MXene film seem to deliver the extremely competitive electrochemical performance when compared with carbon supercapacitors or RuO_2 [147]. PPy/MXene composite seems to deliver a good cycling performance so far due to its self-assembled layered architecture having aligned conductive PPy confined between the conductive $Ti_3C_2T_x$ monolayers. While progress has been made, microsupercapacitor devices are still in its infancy stage and there is a long way to go before they will be commercially available. At present, more effort should be made to construct research roadmaps including arterially designed electrode materials, compatible electrolyte and optimal device architecture, *etc*.

It is of great interest to note that three-electrode swagelok cell should be absolutely sure to collect higher capacitance for corresponding materials than those performed in a two-electrode cell at low current density [46,142]. Therefore, the same type of test device should be adopted to gather comparable electrochemical performance.

3.5. Ion capacitor

Lithium-ion capacitor (Li-IC) is a burgeoning new-concept energy storage device that bridges the gap between rechargeable battery and supercapacitor. Because ion capacitor materials combined the high energy density from the intercalation mechanism of battery and the high power of supercapacitor, *i.e.*, excellent combination of high energy density and power density, they are expected to use in a wide variety of applications such as electric and hybrid cars, mobile electronics devices and sustainable energy storage. As reviewed above, MXenes indeed acted as capacitive electrodes as operated in normal non-aqueous Li/Na-ion battery electrolyte comprising of $LiPF_6$ or $NaPF_6$, thereby MXenes could be regarded as novel Li-ion capacitor materials.

To give play to the large capacity of battery, oxides were strategically introduced into Mxene. Zhang and co-authors reported hierarchical hybrids with T-Nb_2O_5 nanoparticles supported on Nb_2CT_x sheets with disordered carbon, affording a high capacitance of 660 mF cm^{-2} (275F g^{-1}) over charge/discharge times of 4 min and good cycling performance in a nonaqueous lithium electrolyte [159]. The charge storage kinetics are dominated by a surface-controlled process. In another reference [160], the assembled pillared Ti_3C_2 MXene (CTAB-Sn(IV)@Ti_3C_2) exhibited a superior energy density of 239.50 Wh kg^{-1} based on the weight of CTAB-Sn(IV)@Ti_3C_2 under high power density of 10.8 kW kg^{-1} because of the pillar effect (Fig. 10). Sn^{4+} could be successfully anchored onto the alk-Ti_3C_2 by ion-change interaction and electrostatic interactions, effectively confining the occurrence of Sn(IV) detached from the matrix. The possible "pillar effect" of Sn between layers of alk-Ti_3C_2 affirmed in Fig. 10a–d and the synergistic effect between the alk-Ti_3C_2 matrix and Sn enable the nanocomposite to possess outstanding electrochemical properties (Fig. 10e), *e.g.*, a long-term cycling performance of 506 mAh g^{-1} after 250 cycles at a current density of 1 A g^{-1}.

Very recently, as reported by Kajiyama et al. [161], interlayer space of MXene Ti_2CT_x (HF/HCl) expanded to 8.7 Å from 6.8 Å (Fig. 11a). After the initial irreversible SEI formation cycle, the reversible expansion/shrinkage of dinter between 9.8 Å (lithiated) and 9.4 Å (delithiated) could be affirmed upon lithiation/delithiation. The open interlayer space in Ti_2CT_x allowed faster Li-ion diffusion and significantly enhanced Li-ion accessibility of MXene, leading to high gravimetric and volumetric capacitances (300F g^{-1} and 130 F cm^{-3}) (Fig. 11b, c), with less diffusion limitation.

Above electrochemical performance of half-cells has enabled MXene to be a promising candidate for Li-ion capacitor. Therefore, full-cell performance of MXene Li/Na ion capacitor was also investigated to highlight its remarkable application potential.

Recently, full hybrid capacitor aroused concerns from the scientific community. In a reference published in 2015 [162], activated Ti_2CT_x

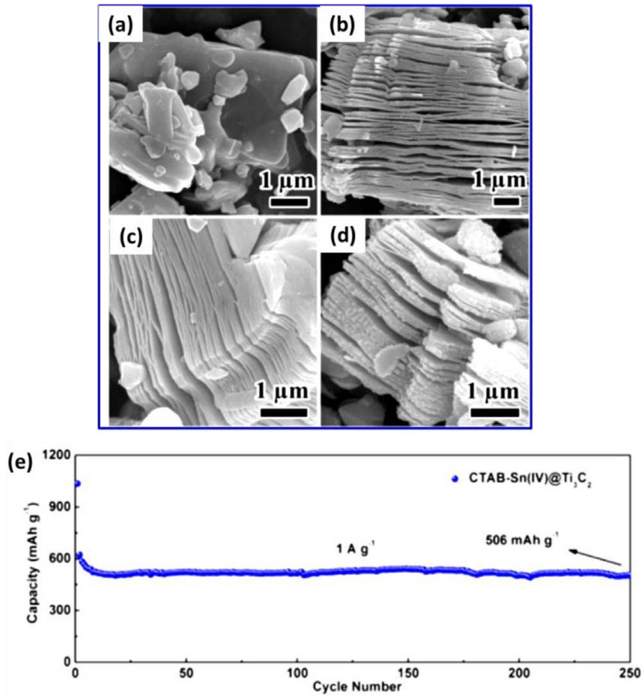

Fig. 10. (a) SEM image of Ti_3AlC_2. (b, c) SEM images of freeze-dried Ti_3C_2. (d) SEM image of oven-dried Ti_3C_2. (e) Long cycling performance of CTAB – Sn(IV)@Ti_3C_2 at a current density of 1 A g^{-1}. Reproduced with permission from Ref. [160] Copyright 2017. American Chemical Society.

was believed to allow reversible Na^+ intercalation/deintercalation into the interlayer space as well as reversible Na^+ adsorption/desorption onto the surface of every layer/sheet (Fig. 11d). Subsequently, the prototype Na-ion full hybrid capacitor with an alluaudite $Na_2Fe_2(SO_4)_3$ positive electrode and a MXene Ti_2C negative electrode operated at a relatively high voltage of 2.4 V was assembled (Fig. 11e) [162], delivering capacities of 90 and 40 mAh g^{-1} at 1.0 and 5.0 A g^{-1} (Fig. 11e–h), respectively. In another reference, the volumetric energy densities of 50–70 Wh L^{-1} for Nb_2CT_x-CNT/$LiFePO_4$ and lithiated Nb_2CT_x-CNT/Nb_2CT_x-CNT cells have been reported to exceed the energy density of a conventional lithium titanium oxide/activated carbon capacitors [107], suggesting a great potential of MXenes in Li-ion capacitors and related energy storage devices.

Very recently, a Li-ion hybrid capacitor consisting of the Ti_2CT_x negative electrode and the $LiNi_{1/3}Co_{1/3}Mn_{1/3}O_2$ positive electrode displayed an unprecedented specific energy density of 160 W h kg^{-1} at 220 W kg^{-1} [161]. An intriguing research has been performed on 2D vanadium carbide of V_2C, affording a Na storage capacitance of similar to 100 F g^{-1} at 0.2 mV s^{-1} [125]. Assembled full cell rendered a capacity of 50 mAh g^{-1} with a cell voltage of 3.5 V when hard carbon was utilized as negative electrode.

In summary, MXenes were generally targeted as pseudocapacitor electrode, which allows Li/Na-ion hybrid capacitors to be liberated from the trade-off between high energy and high power [162]. The enhanced electrochemical performance was ascribed to the intrinsic pseudocapacitive response and energy storage capability of oxides such as Nb_2O_5 or SnO_2 coupled with the fast charge transfer pathways provided by the conductive 2D MXene sheets.

3.6. Hydrogen storage

Hydrogen storage is attracting a lot of interest recently as energy storage in most essential technologies for the development of hydrogen vehicles. Hydrogen gas is considered an ideal fuel for many considerations because of its abundance, efficiency, and highest energy density per unit mass. Although the idea of hydrogen-fuel storage was suggested in early 1972 [163], safety considerations became an obstacle for their wide applications in hydrogen powered vehicles and other applications. Most technologies are used for hydrogen storage in high-pressure or liquid cryogenic tanks.

However, these methods limit their practical applications for commercial use. Recently, a lot of efforts have been tried to find more safe approach through storing hydrogen by adsorbing inside solid state materials such as carbon-based materials [164,165], metal-organic framework (MOFs) and covalent organic frameworks (COFs) materials [166,167]. However, strong bonding between hydrogen atoms and host materials or weak binding force of these materials with hydrogen became a main obstacle for hydrgogen chemisorption or physisorption, respectively, which limits their practical applications of such materials in hydrogen storage devices.

Recently, MXene family showed a great potential for hydrogen storage applications. Hu et al. [168,169] used first principles calculations to investigate the capacity of H_2 adsorption for Ti_2C, Sc_2C, and V_2C structures. The calculations on Ti_2C exhibited that hydrogen could be adsorbed on both sides of Ti_2C layered structure, with the maximum hydrogen capacity of 8.6 wt% [168]. There existed three adsorption modes, *i.e.*, chemisorption of H atom (1.7 wt%), physisorption of H_2 molecule (3.4 wt%) and Kubas-type binding for H_2 molecule (3.4 wt%), accompanying with binding energies of 5.027, 0.109, and 0.272 eV, respectively. Sc_2C and V_2C MXene phases displayed similar hydrogen storage properties as Ti_2C, Which further asserted the potential of the MXene family as hydrogen storage materials.

In 2016, Yadav et al. [170] studied the hydrogen storage capacity for Cr_2C MXene phase, where adsorption sites for reversible H_2 adsorption at ambient conditions were considered with binding energy in the range of 0.1 to 0.4 eV/H_2. The H_2 gravimetric storage capacity for Cr_2C was 7.6 wt% which classified into: chemisorption of H atom (1.2 wt%), Kubas-type binding for H_2 molecule (3.2 wt%), and weak electrostatic interaction of (3.2 wt%) (Fig. 12). All the above mentioned reports suggested that Sc, Ti, and V based MXene materials have greater gravimetric storage capacity than the 2017 DoE recommended target value of 5.5 wt%. As reported by Wu et al. [171], introduction of 2D Ti_3C_2 MXene into $NaAlH_4$ could enhance its hydrogen storage properties. NaAlH4-7 wt% Ti_3C_2 released about 4.7 wt% hydrogen within 100 min at 140 °C, and 4.6 wt% hydrogen could be absorbed into dehydrogenated sample within 1 h at 120 °C. In 2017, the pronounced electrocatalytic activity of MoS_2/Ti_3C_2-MXene@C electrocatalyst was verified by Wu et al. [84], manifesting that HER is catalyzed by such a electrocatalyst by VolmerHeyrovsky mechanism, accompanied with an exchange current density of 29 μA cm^{-2}, higher than that of Pt/C (11 μA cm^{-2}).

In summary, the research into hydrogen storage is still in its infancy. More efforts need to be devoted to revealing the storage mechanism in the aim of the improvement of hydrogen storage capacity.

4. Conclusions and outlook

To date, the increasing interest has been paid to a type of new-concept MXene material, reminiscent of the golden age of graphene. MXene possessed surprising diversity of physical and chemical characteristics, which provided most important opportunities for emerging energy applications, particularly heavy-duty energy storage devices. Although the significant progresses have been made in the most dynamic area, this is still a long way from developing new-concept MXene materials that work in practical energy storage devices.

MXene-based energy storage devices, including rechargeable battery, supercapacitor and ion capacitor (Table 2), are still in the infancy stage so far, and need to be drastically improved. $Nb_4C_3T_x$/Nb_2O_5 afforded a low reversible capacity of 208 mAh g^{-1}@50 mA g^{-1} (0.25 °C) for Li-ion battery, with 94% retention after 400 cycles. As a sodium ion battery material, it is very difficult for MXenes to compete with other

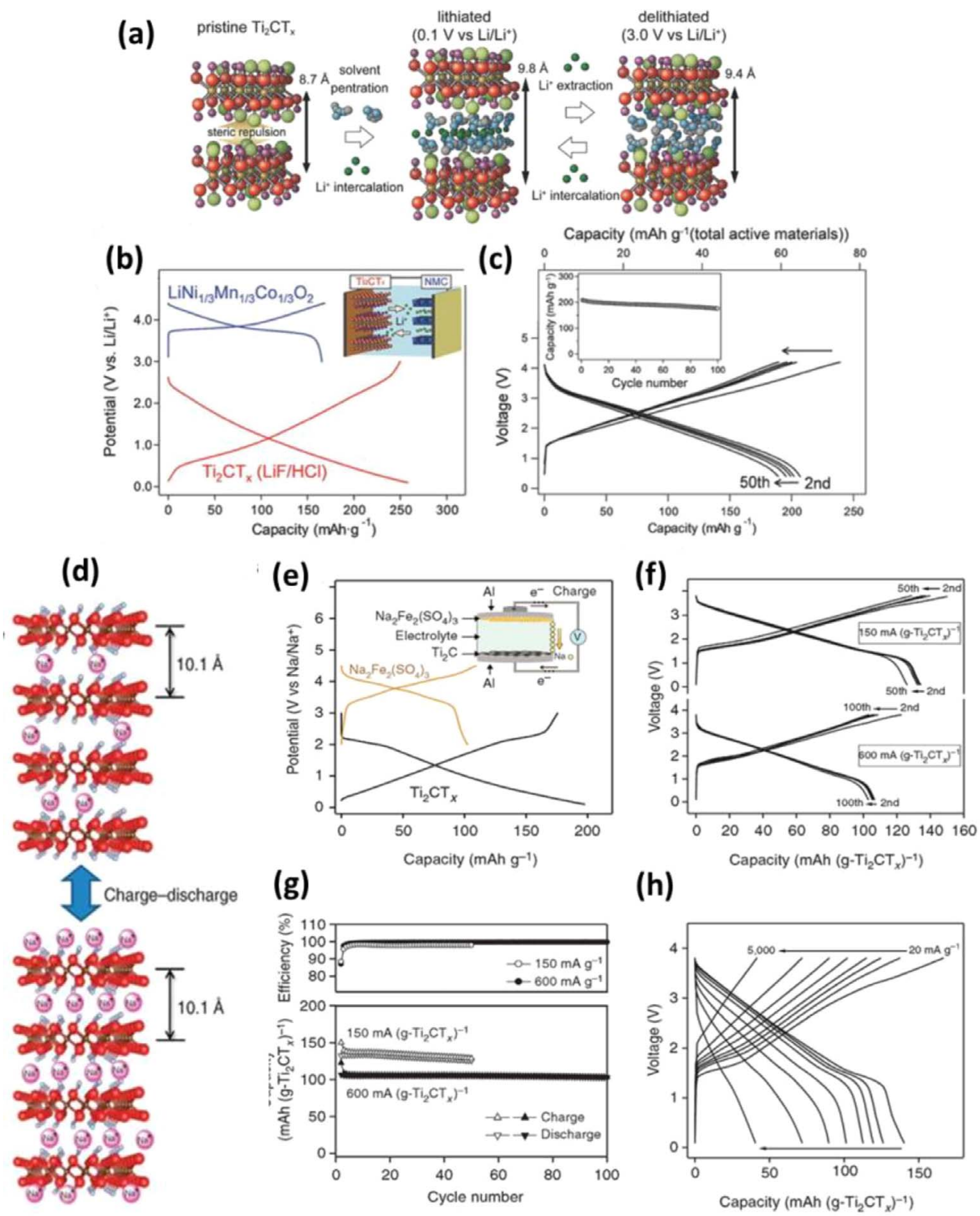

Fig. 11. (a) Reaction mechanism of MXene Ti_2CT_x as Li-ion capacitor material. (b) Charge–discharge curves of Ti_2CT_x and $LiNi_{1/3}Mn_{1/3}Co_{1/3}O_2$ versus Li/Li^+. The inset is a schematic illustration for the Ti_2CT_x-$LiNi_{1/3}Mn_{1/3}Co_{1/3}O_2$ full cell of the Li-ion hybrid capacitor. (c) Charge/discharge curves and cycle performance (inset) of the Ti_2CT_x (LiF/HCl)–$LiNi_{1/3}Mn_{1/3}Co_{1/3}O_2$ Li-ion hybrid capacitor at a specific current of 300 mA·(g of $Ti_2CT_x)^{-1}$. Reproduced with permission from Ref. [161] Copyright 2017. John Wiley & Sons. (d) Schematic illustration of the reaction mechanism of Ti_2CT_x as Na-ion capacitor materials. (e) Charge/discharge curves of Ti_2CT_x and alluaudite $Na_2Fe_2(SO_4)_3$ versus Na/Na^+; the specific currents are 30 and 6 mA g^{-1}, respectively. The inset is a schematic illustration of the Ti_2CT_x alluaudite $Na_2Fe_2(SO_4)_3$ full cell. (f) Voltage profile of the Ti_2CT_x alluaudite $Na_2Fe_2(SO_4)_3$ full cell at the specific currents of 150 and 600 mA (g-$Ti_2CT_x)^{-1}$. (g) Cycle stability and Coulombic efficiency of the full cell with cutoff voltages in the range of 0.1–3.8 V at rates of 150 and 600 mA (g-$Ti_2CT_x)^{-1}$. (h) Charge/discharge profiles at various rates. Reproduced with permission from Ref. [162] Copyright 2015. Macmillan publishers Limited.

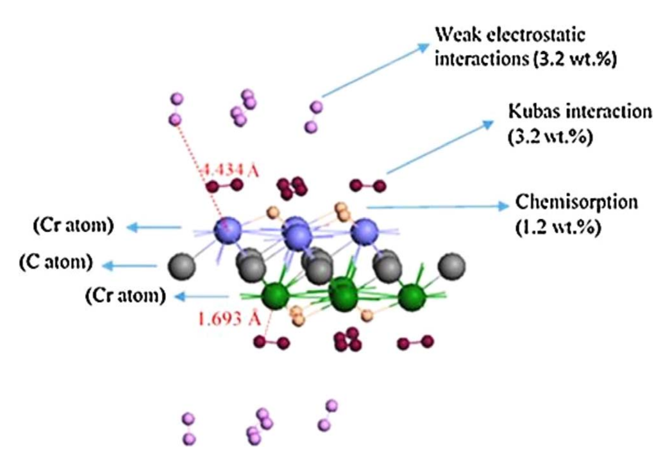

Fig. 12. Graphical representation for adsorption modes of H atoms with Cr_2C Mxene phase. Reproduced with permission from Ref. [170] Copyright 2016. Elsevier B.V.

materials such oxides because of low capacity of 345 mAh cm^{-3}@ 100 mA g^{-1} after 500 cycles. As a supercapacitor materials, $Ti_3C_2T_x$ MXene layers gave a volumetric capacitance of 1000–1500 F cm^{-3}, reaching the previously unmatched volumetric performance of RuO_2. However, researches into ion capacitor were fairly lacking. As full hybrid capacitor, the MXene-based materials afforded a promising electrochemical performance at high power density as compared with the commercial graphite or lithium titanate. However, long-term cycling stability was highly desirable for practice application. Relevant basic research regions will mainly include materials synthesis, device assembly, test system, and more importantly, electrochemical mechanism for realizing the goals of scalable applications.

As to MXenes themselves, two issues need to be noted specially.

(1) MXenes were generally collected by etching MAX phase to remove main group element such as Al or Si. Therefore, it is of extreme difficulty in exactly identifying the details of surface termination groups on MXene even though many testing methods such as XRD, EDS, XPS and NMR have been utilized. In fact, our understanding for the surface/interface chemistry of MXenes is fairly lacking until

Table 2
Typical electrochemical performances of MXene materials for energy storage devices.

Device	Composition	Synthesis approach	Performance	Ref.
Li-ion battery	Nb_2CT_x/10%CNT paper	Filtration	420 mAh g^{-1}@0.5C, ~100% retention after 100 cycles	[36]
	Mo_2CTx-CNT paper	Filtration	250 mAh g^{-1}@ 5 A g^{-1}, 75 mAh g^{-1}@10 mA g^{-1} after 10,000 cycles	[50]
	PVP-Sn(IV)-modified Ti_3C_2	Liquid-phase immersion process	544 mAh g^{-1}@500 mA g^{-1} (1.75C), 94.3% retention after 200 cycles	[99]
	$Nb_4C_3T_x/Nb_2O_5$	One-step CO_2 oxidation	208 mAh g^{-1}@50 mA g^{-1} (0.25C), 94% retention after 400 cycles	[112]
Na-ion battery	Porous $Ti_3C_2T_x$/CNT	Filtration	345 mAh cm^{-3}@100 mA g^{-1}, ~100% retention after 500 cycles	[120]
	Mo_2CTx-CNT paper	Filtration	700 F cm^{-3} (196F g^{-1}) at 2 mV s^{-1}, 100% capacitance retention after 10,000 cycles at 10 A g^{-1}	[50]
Supercapacitor	Clay-like Ti_3C_2 MXene	Filtration	25 mF cm^{-2}@ 2 mA cm^{-2}, 92% retention after 10,000 cycles	[143]
	PPy/$Ti_3C_2T_x$ film	Filtration	1000 F cm^{-3} @5 mV s^{-1}, 92% capacitance retention after 25 000 cycles	[155]
Ion capacitor	CTAB-Sn(IV)@Ti_3C_2	Filtration	33F g^{-1}@2 A g^{-1}, 71.7% retention after 4000 cycles at 2 A g^{-1}	[160]
	Nb_2O_5/Nb_2CT_x	One-step CO_2 oxidation	660 mF cm^{-2} (275F g^{-1}) over a charge–discharge time of 4 min	[159]
Full hybrid capacitor	Cathode: $LiFePO_4$ Anode: Nb_2CT_x/CNT		50–70 Wh L^{-1}	[107]
	Cathode: $LiNi_{1/3}Co_{1/3}Mn_{1/3}O_2$ Anode: Ti_2CT_x		160 W h kg^{-1} at 220 W kg^{-1}	[161]

now. Now, theoretical simulation is still considered as essential route to gain an insight into relation between performance and structure. However, as a real material for energy application, the experimental results are of vital importance in verifying those theoretical evaluations.

(2) MXenes possessed some distinctive features such as rigid structure, large molar mass and very limited ratio of horizontal/vertical direction as compared with graphene. Even though it becomes almost impossible to cover, wrap or coat those solid particles such as oxides or sulfides for MXene because it is not constitutionally flexible or elastic, there existed an opportunity to provide a pillared structure for hosting the nanoparticles, whereby architectural consistency of MXene-based materials should be robustly preserved during cycling. In other words, enlarged interlayer spacing enables chemical reaction to set off between interlayers without structure damage, implying we could intercalate designed compounds with expectant morphology and microstructure into interlayers as the electrochemically active materials.

As to rechargeable batteries, tremendous efforts will be required for the development of new-concept MXene materials and their hybrids with abundant functional groups and ample microstructures. Such a MXene will be further utilized to make components for electrodes featuring a high storage capacity, an improved columbic efficiency and a long cycling life. For LIBs or SIBs, there existed still a controversy for MXenes in regard to the actual lithiation reaction during charging/discharging processes because recent mechanism on absorption-desorption is very different with the traditional theories such as intercalation, alloying and conversion. As to SIBs, low capacity and poor rate capability of anodes are formidable bottlenecks to be handled. As to supercapacitor, large volumetric expansion during intercalation may require MXenes layers pillaring with polymers or small molecules before MXenes can be actually served as capacitor electrodes.

To display the unique characteristic of MXene, ion capacitor with high energy density and power density should be a very promising device in the near future. Several problems are here raised and possible solutions are also listed for discussion and reference.

(1) It appears to be difficult to theoretically simulate the exact contribution and essential origin of capacitance or battery for the new-concept device of ion capacitor until now. Theoretical simulation will be still proven as a strong tool to understand the root cause of electrochemical performance.
(2) Recent investigations into ion capacitor focus their attention on Sn (IV) (possible SnO_2) and Nb_2O_5 nanoparticles. More oxides and sulfides should be developed to widen the research region in order to look for more suitable intercalated compounds with a controllable content and microstructure. For instance, sol-gel technique, the controllable hydrolysis of the transition metal salts, and hydrothermal route will be viable approach to form oxides between the interlayers of MXene, further, oxides can be converted into sulfides *via* a sulfurization technology. Thus, we can largely extend our inorganic compound family as intercalants of MXenes, *i.e.*, active materials for energy storage.
(3) Development of efficient, stable, and cost-effective electrolyte systems is of high emergency, because almost all electrolytes are specifically made up for the graphite-based Li-ion battery so far. Influence of operational voltage on overall electrochemical performance such as gravimetric energy density and power density is observably important. Thus, exploitation of electrolyte with a high operational voltage window becomes of realistic importance.
(4) Interfacial features of MXene immersed in electrolyte exercised a crucial influence over electrochemical performance. At present, related basic researches on solid/liquid interface is almost completely lacking, and needs to be launched.
(5) To properly compare the results, more standard test system will be forethoughtfully exploited based on current two- and three-electrode configurations for establishing uniform scientific standards and promoting the academic communications among different research groups.

Scalable layered materials with low cost, high efficiency and environmental friendliness are the most factors for the practical application of energy storage devices. Thus, suitable strategy is of high urgency in producing high quality MXene in a controllable way. Different microstructures such as sandwich-like structure and 3D hybrid structures should be well-designed to produce desirable specific surface area, pore sizes, and pore size distribution. The artificially designed nanostructures possess great potential to address some essential issues appeared in electrochemical reaction of MXene during cycling, tremendously improving the reversible capacity and cycle life of corresponding devices.

Although significant researches have been performed so far, much effort should be further devoted to revealing the relations between structure–electrochemical property. From a practical perspective, there is a huge gap between reality and dream. Based on the balance between reasonable costs with acceptable performance, MXenes have a long way to go before they are utilized as electrode materials for commercial energy storage devices. Therefore, in-depth basic researches are extremely needed. On other hand, a close collaboration will be efficiently carried out between the government, academia, and industry to deal with all kinds of complicated problems, which will appear in full life cycle development process of MXene-based materials from the laboratory bench, the factory machine, and finally to the consumer's hand. We entirely believe that there will be a bright future for MXene as energy storage materials after some fundamental difficulties, such as material synthesis, design of electrode structures, the compatibility of electrolyte, and more importantly charge storage mechanisms, *etc*, are gradually handled based on both experimental and theoretical assessments.

Conflicts of interest

There are no conflicts to declare.

Acknowledgements

This work is supported by the Department of Science and Technology of Guangdong (Nos. 2014B010123001, 2015B090901030, and 2016B050502004), Guangzhou Science Technology and Innovation Commission (No. 2016201604030013), and Bureau of Science and Technology of Foshan Municipality (No. 2016AG100522).

Appendix A. Supplementary data

Supplementary data associated with this article can be found, in the online version, at http://dx.doi.org/10.1016/j.cej.2017.12.155.

References

[1] M.M. Hoque, M.A. Hannan, A. Mohamed, A. Ayob, Battery charge equalization controller in electric vehicle applications: a review, Renew. Sustain. Energy Rev. 75 (2017) 1363–1385.
[2] A. Jaiswal, Lithium-ion battery based renewable energy solution for off-grid electricity: a techno-economic analysis, Renew. Sustain. Energy Rev. 72 (2017) 922–934.
[3] E. Telaretti, L. Dusonchet, Stationary battery technologies in the US: development trends and prospects, Renew. Sustain. Energy Rev. 75 (2017) 380–392.
[4] S. Zheng, X. Li, B. Yan, Q. Hu, Y. Xu, X. Xiao, H. Xue, H. Pang, Transition-metal (Fe Co, Ni) based metal-organic frameworks for electrochemical energy storage, Adv. Energy Mater. 7 (2017) 1602733.
[5] Y. Lu, B. Li, S. Zheng, Y. Xu, H. Xue, H. Pang, Syntheses and energy storage applications of M_xS_y (M = Cu, Ag, Au) and their composites: rechargeable batteries and supercapacitors, Adv. Funct. Mater. 27 (2017) 1703949.
[6] X. Zhang, Z. Zhang, Z. Zhou, MXene-based materials for electrochemical energy storage, J. Energy Chem. 27 (2018) 73–85.
[7] S. Zheng, H. Xue, H. Pang, Supercapacitors based on metal coordination materials, Coord. Chem. Rev. (2017), http://dx.doi.org/10.1016/j.ccr.2017.1007.1002.
[8] X. Li, S. Ding, X. Xiao, J. Shao, J. Wei, H. Pang, Y. Yu, N, S co-doped 3D mesoporous carbon–$C_o3S_i2_O5(OH_)4$ architectures for high-performance flexible pseudo-solid-state supercapacitors, J. Mater. Chem. A 5 (2017) 12774–12781.
[9] B. Li, P. Gu, Y. Feng, G. Zhang, K. Huang, H. Xue, H. Pang, Ultrathin nickel-cobalt phosphate 2D nanosheets for electrochemical energy storage under aqueous/solid-state electrolyte, Adv. Funct. Mater. 27 (2017) 1605784.
[10] S. Wu, R. Xu, M. Lu, R. Ge, J. Iocozzia, C. Han, B. Jiang, Z. Lin, Graphene-containing nanomaterials for lithium-ion batteries, Adv. Energy Mater. 5 (2015) 1500400.
[11] S. Wu, R. Ge, M. Lu, R. Xu, Z. Zhang, Graphene-based nano-materials for lithium–sulfur battery and sodium-ion battery, Nano Energy 15 (2015) 379–405.
[12] X. Guo, S. Zheng, G. Zhang, X. Xiao, X. Li, Y. Xu, H. Xue, H. Pang, Nanostructured graphene-based materials for flexible energy storage, Energy Storage Mater. 9 (2017) 150–169.
[13] S. Wu, Y. Du, S. Sun, Transition metal dichalcogenide based nanomaterials for rechargeable batteries, Chem. Eng. J. 307 (2017) 189–207.
[14] G. Zhang, X. Xiao, B. Li, P. Gu, H. Xue, H. Pang, Transition metal oxides with one-dimensional/one-dimensional-analogue nanostructures for advanced supercapacitors, J. Mater. Chem. A 5 (2017) 8155–8186.
[15] X. Zhang, L. Hou, A. Ciesielski, P. Samorì, 2D materials beyond graphene for high-performance energy storage applications, Adv. Energy Mater. 6 (2016) 1600671.
[16] F. Wang, C. Yang, M. Duan, Y. Tang, J. Zhu, TiO_2 nanoparticle modified organ-like Ti_3C_2 MXene nanocomposite encapsulating hemoglobin for a mediator-free biosensor with excellent performances, Biosens. Bioelectron. 74 (2015) 1022–1028.
[17] H. Liu, C. Duan, C. Yang, W. Shen, F. Wang, Z. Zhu, A novel nitrite biosensor based on the direct electrochemistry of hemoglobin immobilized on MXene-Ti_3C_2, Sens. Actuators, B 218 (2015) 60–66.
[18] M.D. Levi, M.R. Lukatskaya, S. Sigalov, M. Beidaghi, N. Shpigel, L. Daikhin, D. Aurbach, M.W. Barsoum, Y. Gogotsi, Solving the capacitive paradox of 2D MXene using electrochemical quartz-crystal admittance and in situ electronic conductance measurements, Adv. Energy Mater. 5 (2015) 1400815.
[19] J.C. Lei, X. Zhang, Z. Zhou, Recent advances in MXene: preparation, properties, and applications, Front. Phys. 10 (2015) 276–286.
[20] Y. Yoon, K. Lee, H. Lee, Low-dimensional carbon and MXene-based electrochemical capacitor electrodes, Nanotechnology 27 (2016) 172001.
[21] L. Peng, Y. Zhu, H. Li, G. Yu, Chemically integrated inorganic-graphene two-dimensional hybrid materials for flexible energy storage devices, Small 12 (2016) 6183–6199.
[22] L. Peng, Y. Zhu, D. Chen, R.S. Ruoff, G. Yu, Two-dimensional materials for beyond-lithium-ion batteries, Adv. Energy Mater. 6 (2016) 1600025.
[23] Y. Sun, D. Chen, Z. Liang, Two-dimensional MXenes for energy storage and conversion applications, Mater. Today Energy 5 (2017) 22–36.
[24] B. Anasori, M.R. Lukatskaya, Y. Gogotsi, 2D metal carbides and nitrides (MXenes) for energy storage, Nat. Rev. Mater. 2 (2017) 16098.
[25] K. Chen, D. Xue, Nanofabrication strategies for advanced electrode materials, Nanofabrication (2017) 1.
[26] M. Alhabeb, K. Maleski, B. Anasori, P. Lelyukh, L. Clark, S. Sin, Y. Gogotsi, Guidelines for synthesis and processing of two-dimensional titanium carbide (Ti_3C_2TX MXene), Chem. Mater. 29 (2017) 7633–7644.
[27] F. Wang, Z. Wang, J. Zhu, H. Yang, X. Chen, L. Wang, C. Yang, Facile synthesis SnO_2 nanoparticle-modified Ti_3C_2 MXene nanocomposites for enhanced lithium storage application, J. Mater. Sci. 52 (2017) 3556–3565.
[28] Y. Tian, C. Yang, W. Que, Y. He, X. Liu, Y. Luo, X. Yin, L.B. Kong, Ni foam supported quasi-core-shell structure of ultrathin Ti_3C_2 nanosheets through electrostatic layer-by-layer self-assembly as high rate-performance electrodes of supercapacitors, J. Power Sources 369 (2017) 78–86.
[29] Y. Wu, P. Nie, L. Wu, H. Dou, X. Zhang, 2D MXene/SnS_2 composites as high-performance anodes for sodium ion batteries, Chem. Eng. J. 334 (2018) 932–938.
[30] L. Feng, X.H. Zha, K. Luo, Q. Huang, J. He, Y.J. Liu, W. Deng, S.Y. Du, Structures and mechanical and electronic properties of the Ti_2CO_2 MXene incorporated with neighboring elements (Sc, V, B and N), J. Electron. Mater. 46 (2017) 2460–2466.
[31] X. Zhang, X. Zhao, D. Wu, J. Yu, Z. Zhou, High and anisotropic carrier mobility in experimentally possible Ti_2CO_2 (MXene) monolayers and nanoribbons, Nanoscale 7 (2015) 16020.
[32] K.J. Harris, M. Bugnet, M. Naguib, M.W. Barsoum, G.R. Goward, Direct measurement of surface termination groups and their connectivity in the 2D MXene V_2CT_x using NMR spectroscopy, J. Phys. Chem. C 119 (2015) 13713–13720.
[33] Y. Zhang, F. Li, Robust half-metallic ferromagnetism in Cr_3C_2 MXene, J. Magn. Magn. Mater. 433 (2017) 222–226.
[34] Y.L. Yue, Fe_2C monolayer: an intrinsic ferromagnetic MXene, J. Magn. Magn. Mater. 434 (2017) 164–168.
[35] M. Ghidiu, M. Naguib, C. Shi, O. Mashtalir, L.M. Pan, B. Zhang, J. Yang, Y. Gogotsi, S.J.L. Billinge, M.W. Barsoum, Synthesis and characterization of two-dimensional Nb_4C_3 (MXene), Chem. Commun. 50 (2014) 9517–9520.
[36] O. Mashtalir, M.R. Lukatskaya, M.-Q. Zhao, M.W. Barsoum, Y. Gogotsi, Amine-Assisted delamination of Nb_2C MXene for Li-ion energy storage devices, Adv. Mater. 27 (2015) 3501–3506.
[37] Q.Z. Tao, M. Dahlqvist, J. Lu, S. Kota, R. Meshkian, J. Halim, J. Palisaitis, L. Hultman, M.W. Barsoum, P.O.A. Persson, J. Rosen, Two-dimensional $Mo_{1.33}C$ MXene with divacancy ordering prepared from parent 3D laminate with in-plane chemical ordering, Nat. Commun. 8 (2017) 14949.
[38] J.C. Lei, A. Kutana, B.I. Yakobson, Predicting stable phase monolayer Mo_2C (MXene), a superconductor with chemically-tunable critical temperature, J. Mater. Chem. C 5 (2017) 3438–3444.
[39] C. Zhao, C. Yu, M. Zhang, H. Huang, S. Li, X. Han, Z. Liu, J. Yang, W. Xiao, J. Liang, X. Sun, J. Qiu, Ultrafine MoO_2-carbon microstructures enable ultralong-life power-type sodium ion storage by enhanced pseudocapacitance, Adv. Energy Mater. (2017) 1602880.
[40] D.D. Sun, Q.K. Hu, J.F. Chen, X.Y. Zhang, L.B. Wang, Q.H. Wu, A.G. Zhou, Structural transformation of MXene (V_2C, Cr_2C, and Ta_2C) with O groups during lithiation: a first-principles investigation, ACS Appl. Mater. Interfaces 8 (2016) 74–81.
[41] G. Wang, Theoretical prediction of the intrinsic half-metallicity in surface-oxygen-passivated Cr_2N MXene, J. Phys. Chem. C 120 (2016) 18850–18857.
[42] P. Urbankowski, B. Anasori, T. Makaryan, D.Q. Er, S. Kota, P.L. Walsh, M.Q. Zhao, V.B. Shenoy, M.W. Barsoum, Y. Gogotsi, Synthesis of two-dimensional titanium nitride Ti_4N_3 (MXene), Nanoscale 8 (2016) 11385–11391.
[43] C. Shi, M. Beidaghi, M. Naguib, O. Mashtalir, Y. Gogotsi, S.J.L. Billinge, Structure of nanocrystalline Ti_3C_2 MXene using atomic pair distribution function, Phys. Rev. Lett. 112 (2014) 125501.
[44] M.R. Lukatskaya, O. Mashtalir, C.E. Ren, Y. Dall'Agnese, P. Rozier, P.L. Taberna, M. Naguib, P. Simon, M.W. Barsoum, Y. Gogotsi, Cation intercalation and high volumetric capacitance of two-dimensional titanium carbide, Science 341 (2013) 1502–1505.
[45] M.-Q. Zhao, C.E. Ren, Z. Ling, M.R. Lukatskaya, C. Zhang, K.L. Van Aken, M.W. Barsoum, Y. Gogotsi, Flexible MXene/carbon nanotube composite paper with high volumetric capacitance, Adv. Mater. 27 (2015) 339–345.
[46] R.B. Rakhi, B. Ahmed, M.N. Hedhili, D.H. Anjum, H.N. Alshareef, Effect of post-etch annealing gas composition on the structural and electrochemical properties of Ti_2CT_x MXene electrodes for supercapacitor applications, Chem. Mater. 27 (2015) 5314–5323.
[47] Z. Ma, Z. Hu, X. Zhao, Q. Tang, D. Wu, Z. Zhou, L. Zhang, Tunable band structures of heterostructured bilayers with transition-metal dichalcogenide and MXene mono layer, J. Phys. Chem. C 118 (2014) 5593–5599.

[48] E. Balci, U.O. Akkus, S. Berber, Band gap modification in doped MXene: Sc_2CF_2, J. Mater. Chem. C 5 (2017) 5956–5961.
[49] X. Zhang, Z. Ma, X. Zhao, Q. Tang, Z. Zhou, Computational studies on structural and electronic properties of functionalized MXene monolayers and nanotubes, J. Mater. Chem. A 3 (2015) 4960–4966.
[50] J. Halim, S. Kota, M.R. Lukatskaya, M. Naguib, M.-Q. Zhao, E.J. Moon, J. Pitock, J. Nanda, S.J. May, Y. Gogotsi, M.W. Barsoum, Synthesis and characterization of 2D molybdenum carbide (MXene), Adv. Funct. Mater. 26 (2016) 3118–3127.
[51] K. Hantanasirisakul, M.-Q. Zhao, P. Urbankowski, J. Halim, B. Anasori, S. Kota, C.E. Ren, M.W. Barsoum, Y. Gogotsi, Fabrication of Ti_3C_2Tx MXene transparent thin films with tunable optoelectronic properties, Adv. Electron. Mater. 2 (2016) 1600050.
[52] Y. Ando, S. Watanabe, First-principles study of metal-insulator control by ion adsorption on Ti_2C MXene dioxide monolayers, Appl. Phys Express 9 (2016) 015001.
[53] A. Miranda, J. Halim, M.W. Barsoum, A. Lorke, Electronic properties of free-standing $Ti_3C_2T_x$ MXene monolayers, Appl. Phys. Lett. 108 (2016) 033102.
[54] B. Aissa, A. Ali, K.A. Mahmoud, T. Haddad, M. Nedil, Transport properties of a highly conductive 2D $Ti_3C_2T_x$ MXene/graphene composite, Appl. Phys. Lett. 109 (2016) 043109.
[55] X. Sang, Y. Xie, M.-W. Lin, M. Alhabeb, K.L. Van Aken, Y. Gogotsi, P.R.C. Kent, K. Xiao, R.R. Unocic, Atomic defects in monolayer titanium carbide ($Ti_3C_2T_x$) MXene, Acs Nano 10 (2016) 9193–9200.
[56] J. Chen, K. Chen, D. Tong, Y. Huang, J. Zhang, J. Xue, Q. Huang, T. Chen, CO_2 and temperature dual responsive "Smart'" MXene phases, Chem. Commun. 51 (2015) 314–317.
[57] H. Wang, Y. Wu, J. Zhang, G. Li, H. Huang, X. Zhang, Q. Jiang, Enhancement of the electrical properties of MXene Ti_3C_2 nanosheets by post-treatments of alkalization and calcination, Mater. Lett. 160 (2015) 537–540.
[58] J. Yan, C.E. Ren, K. Maleski, C.B. Hatter, B. Anasori, P. Urbankowski, A. Sarycheva, Y. Gogotsi, Flexible MXene/graphene films for ultrafast supercapacitors with outstanding volumetric capacitance, Adv. Funct. Mater. 27 (2017) 1701264.
[59] Z. Ling, C.E. Ren, M.-Q. Zhao, J. Yang, J.M. Giammarco, J. Qiu, M.W. Barsoum, Y. Gogotsi, Flexible and conductive MXene films and nanocomposites with high capacitance, PNAS 111 (2014) 16676–16681.
[60] Y. Xie, M. Naguib, V.N. Mochalin, M.W. Barsoum, Y. Gogotsi, X. Yu, K.-W. Nam, X.-Q. Yang, A.I. Kolesnikov, P.R.C. Kent, Role of surface structure on Li-Ion energy storage capacity of two-dimensional transition-metal carbides, J. Am. Chem. Soc. 136 (2014) 6385–6394.
[61] T. Liang, M. Ashton, K. Choudhary, D. Zhang, A.F. Fonseca, B.C. Revard, R.G. Hennig, S.R. Phillpot, S.B. Sinnott, Properties of Ti/TiC interfaces from molecular dynamics simulations, J. Phys. Chem. C 120 (2016) 12530–12538.
[62] N.B. Vadym, N.M. Vadym, G. Yury, Molecular dynamic study of the mechanical properties of two-dimensional titanium carbides Ti $_{n+1}$ C $_n$ (MXenes), Nanotechnology 26 (2015) 265705.
[63] X. Xie, S. Chen, W. Ding, Y. Nie, Z. Wei, An extraordinarily stable catalyst: Pt NPs supported on two-dimensional $Ti_3C_2X_2$ (X = OH, F) nanosheets for oxygen reduction reaction, Chem. Commun. 49 (2013) 10112–10114.
[64] F. Wang, C. Yang, C. Duan, D. Xiao, Y. Tang, J. Zhu, An organ-like titanium carbide material (MXene) with multilayer structure encapsulating hemoglobin for a mediator-free biosensor, J. Electrochem. Soc. 162 (2015) B16–B21.
[65] K. Rasool, K.A. Mahmoud, D.J. Johnson, M. Helal, G.R. Berdiyorov, Y. Gogotsi, Efficient antibacterial membrane based on two-dimensional $Ti_3C_2T_x$ (MXene) nanosheets, Sci. Rep. 7 (2017) 1598.
[66] A.K. Fard, G. McKay, R. Chamoun, T. Rhadfi, H. Preud'Homme, M.A. Atieh, Barium removal from synthetic natural and produced water using MXene as two dimensional (2-D) nanosheet adsorbent, Chem. Eng. J. 317 (2017) 331–342.
[67] L. Lorencova, T. Bertok, E. Dosekova, A. Holazova, D. Paprckova, A. Vikartovska, V. Sasinkova, J. Filip, P. Kasak, M. Jerigova, D. Velic, K.A. Mahmoud, J. Tkac, Electrochemical performance of $Ti_3C_2T_x$ MXene in aqueous media: towards ultrasensitive H_2O_2 sensing, Electrochim. Acta 235 (2017) 471–479.
[68] Q. Xue, H.J. Zhang, M.S. Zhu, Z.X. Pei, H.F. Li, Z.F. Wang, Y. Huang, Y. Huang, Q.H. Deng, J. Zhou, S.Y. Du, Q. Huang, C.Y. Zhi, Photoluminescent Ti_3C_2 MXene quantum dots for multicolor cellular imaging, Adv. Mater. 29 (2017) 1604847.
[69] L. Dong, H. Kumar, B. Anasori, Y. Gogotsi, V.B. Shenoy, Rational design of two-dimensional metallic and semiconducting spintronic materials based on ordered double-transition-metal MXenes, J. Phys. Chem. Lett. 8 (2017) 422–428.
[70] G.R. Berdiyorov, Optical properties of functionalized $Ti_3C_2T_2$ (T = F, O, OH) MXene: first-principles calculations, Aip Adv. 6 (2016) 055105.
[71] Z.W. Seh, K.D. Fredrickson, B. Anasori, J. Kibsgaard, A.L. Strickler, M.R. Lukatskaya, Y. Gogotsi, T.F. Jaramillo, A. Vojvodic, Two-dimensional molybdenum carbide (MXene) as an efficient electrocatalyst for hydrogen evolution, ACS Energy Lett. 1 (2016) 589–594.
[72] Z.L. Guo, N.H. Miao, J. Zhou, B.S. Sa, Z. Sun, Strain-mediated type-I/type-II transition in MXene/Blue phosphorene van der Waals heterostructures for flexible optical/electronic devices, J. Mater. Chem. C 5 (2017) 978–984.
[73] M. Ghidiu, M.R. Lukatskaya, M.-Q. Zhao, Y. Gogotsi, M.W. Barsoum, Conductive two-dimensional titanium carbide clay with high volumetric capacitance, Nature 516 (2014) 78–81.
[74] O. Mashtalir, M. Naguib, V.N. Mochalin, Y. Dall'Agnese, M. Heon, M.W. Barsoum, Y. Gogotsi, Intercalation and delamination of layered carbides and carbonitrides, Nat. Commun. 4 (2013) 1716.
[75] P. Srivastava, A. Mishra, H. Mizuseki, K.-R. Lee, A.K. Singh, Mechanistic insight into the chemical exfoliation and functionalization of Ti_3C_2 MXene, ACS Appl. Mater. Interfaces 8 (2016) 24256–24264.
[76] D. Magne, V. Mauchamp, S. Celerier, P. Chartier, T. Cabioc'h, Site-projected electronic structure of two-dimensional Ti_3C_2 MXene: the role of the surface functionalization groups, PCCP 18 (2016) 30946–30953.
[77] Z. Li, L. Wang, D. Sun, Y. Zhang, B. Liu, Q. Hu, A. Zhou, Synthesis and thermal stability of two-dimensional carbide MXene Ti_3C_2, Mater. Sci. Eng. B-Adv. Funct. Solid-State Mater. 191 (2015) 33–40.
[78] T.L. Tan, H.M. Jin, M.B. Sullivan, B. Anasori, Y. Gogotsi, High-throughput survey of ordering configurations in MXene alloys across compositions and temperatures, Acs Nano 11 (2017) 4407–4418.
[79] N.C. Osti, M. Naguib, A. Ostadhossein, Y. Xie, P.R.C. Kent, B. Dyatkin, G. Rother, W.T. Heller, A.C.T. van Duin, Y. Gogotsi, E. Mamontov, Effect of metal ion intercalation on the structure of MXene and water dynamics on its internal surfaces, ACS Appl. Mater. Interfaces 8 (2016) 8859–8863.
[80] A. Vaughn, J. Ball, T. Heil, D.J. Morgan, G.I. Lampronti, G. Marsalkaite, C.L. Raston, N.P. Power, S. Kellici, Selective calixarene-directed synthesis of MXene plates crumpled sheets, spheres, and scrolls, Chem. Eur. J. 23 (2017) 8128–8133.
[81] X. Liang, Y. Rangom, C.Y. Kwok, Q. Pang, L.F. Nazar, Interwoven MXene nanosheet/carbon-nanotube composites as Li-S cathode hosts, Adv. Mater. (Deerfield Beach, Fla.) 29 (2017) 1603040.
[82] P. Simon, Two-dimensional MXene with controlled interlayer spacing for electrochemical energy storage, ACS Nano 11 (2017) 2393–2396.
[83] Q.X. Xia, J. Fu, J.M. Yun, R.S. Mane, K.H. Kim, High volumetric energy density annealed-MXene-nickel oxide/MXene asymmetric supercapacitor, RSC Adv. 7 (2017) 11000–11011.
[84] X. Wu, Z. Wang, M. Yu, L. Xiu, J. Qiu, Stabilizing the MXenes by carbon nanoplating for developing hierarchical nanohybrids with efficient lithium storage and hydrogen evolution capability, Adv. Mater. 29 (2017) 1607017.
[85] M. Khazaei, M. Arai, T. Sasaki, C.-Y. Chung, N.S. Venkataramanan, M. Estili, Y. Sakka, Y. Kawazoe, Novel electronic and magnetic properties of two-dimensional transition metal carbides and nitrides, Adv. Funct. Mater. 23 (2013) 2185–2192.
[86] M. Ashton, K. Mathew, R.G. Hennig, S.B. Sinnoet, Predicted surface composition and thermodynamic stability of MXenes in solution, J. Phys. Chem. C 120 (2016) 3550–3556.
[87] G.R. Berdiyorov, Effect of lithium and sodium ion adsorption on the electronic transport properties of Ti_3C_2 MXene, Appl. Surf. Sci. 359 (2015) 153–157.
[88] G.R. Berdiyorov, M.E. Madjet, K.A. Mahmoud, Ionic sieving through $Ti_3C_2(OH)(_2)$ MXene: first-principles calculations, Appl. Phys. Lett. 108 (2016) 113110.
[89] J. Guo, Q. Peng, H. Fu, G. Zou, Q. Zhang, Heavy-metal adsorption behavior of two-dimensional alkalization-intercalated MXene by first-principles calculations, J. Phys. Chem. C 119 (2015) 20923–20930.
[90] A. Mishra, P. Srivastava, H. Mizuseki, K.-R. Lee, A.K. Singh, Isolation of pristine MXene from Nb_4AlC_3 MAX phase: a first-principles study, PCCP 18 (2016) 11073–11080.
[91] M. Ghidiu, S. Kota, J. Halim, A.W. Sherwood, N. Nedfors, J. Rosen, V.N. Mochalin, M.W. Barsoum, Alkylammonium cation intercalation into Ti_3C_2 (MXene): effects on properties and ion-exchange capacity estimation, Chem. Mater. 29 (2017) 1099–1106.
[92] Q. Tang, Z. Zhou, P. Shen, Are MXenes promising anode materials for Li ion batteries? computational studies on electronic properties and Li storage capability of Ti_3C_2 and $Ti_3C_2X_2$ (X = F, OH) monolayer, J. Am. Chem. Soc. 134 (2012) 16909–16916.
[93] Y.-X. Yu, Prediction of mobility, enhanced storage capacity, and volume change during sodiation on interlayer-expanded functionalized Ti_3C_2 MXene anode materials for sodium-ion batteries, J. Phys. Chem. C 120 (2016) 5288–5296.
[94] L.H. Karlsson, J. Birch, J. Halim, M.W. Barsoum, P.O.A. Persson, Atomically resolved structural and chemical investigation of single MXene sheets, Nano Lett. 15 (2015) 4955–4960.
[95] Y. Xie, Y. Dall'Agnese, M. Naguib, Y. Gogotsi, M.W. Barsoum, H.L. Zhuang, P.R.C. Kent, Prediction and characterization of MXene nanosheet anodes for non-lithium-ion batteries, ACS Nano 8 (2014) 9606–9615.
[96] M. Ghidiu, J. Halim, S. Kota, D. Bish, Y. Gogotsi, M.W. Barsoum, Ion-exchange and cation solvation reactions in Ti_3C_2 MXene, Chem. Mater. 28 (2016) 3507–3514.
[97] Y.Y. Wen, T.E. Rufford, X.Z. Chen, N. Li, M.Q. Lyu, L.M. Dai, L.Z. Wang, Nitrogen-doped $Ti_3C_2T_x$ MXene electrodes for high-performance supercapacitors, Nano Energy 38 (2017) 368–376.
[98] J. Zhou, X. Zha, X. Zhou, F. Chen, G. Gao, S. Wang, C. Shen, T. Chen, C. Zhi, P. Eklund, S. Du, J. Xue, W. Shi, Z. Chai, Q. Huang, Synthesis and electrochemical properties of two-dimensional hafnium carbide, ACS Nano 11 (2017) 3841–3850.
[99] J. Luo, X. Tao, J. Zhang, Y. Xia, H. Huang, L. Zhang, Y. Gan, C. Liang, W. Zhang, Sn^{4+} ion decorated highly conductive Ti_3C_2 MXene: promising lithium-ion anodes with enhanced volumetric capacity and cyclic performance, ACS Nano 10 (2016) 2491–2499.
[100] H. Sun, L. Mei, J. Liang, Z. Zhao, C. Lee, H. Fei, M. Ding, J. Lau, M. Li, C. Wang, X. Xu, G. Hao, B. Papandrea, I. Shakir, B. Dunn, Y. Huang, X. Duan, Three-dimensional holey-graphene/niobia composite architectures for ultrahigh-rate energy storage, Science 356 (2017) 599–604.
[101] M. Ashton, R.G. Hennig, S.B. Sinnott, Computational characterization of lightweight multilayer MXene Li-ion battery anodes, Appl. Phys. Lett. 108 (2016) 023901.
[102] D. Er, J. Li, M. Naguib, Y. Gogotsi, V.B. Shenoy, Ti_3C_2 MXene as a high capacity electrode material for metal (Li, Na, K, Ca) ion batteries, ACS Appl. Mater. Interfaces 6 (2014) 11173–11179.
[103] X. Chen, Z. Kong, N. Li, X. Zhao, C. Sun, Proposing the prospects of Ti_3CN transition metal carbides (MXenes) as anodes of Li-ion batteries: a DFT study, PCCP 18

(2016) 32937–32943.
[104] S.J. Kim, M. Naguib, M. Zhao, C. Zhang, H.-T. Jung, M.W. Barsoum, Y. Gogotsi, High mass loading, binder-free MXene anodes for high areal capacity Li-ion batteries, Electrochim. Acta 163 (2015) 246–251.
[105] F. Du, H. Tang, L. Pan, T. Zhang, H. Lu, J. Xiong, J. Yang, C. Zhang, Environmental friendly scalable production of colloidal 2D titanium carbonitride MXene with minimized nanosheets restacking for excellent cycle life lithium-ion batteries, Electrochim. Acta 235 (2017) 690–699.
[106] S. Zhao, X. Meng, K. Zhu, F. Du, G. Chen, Y. Wei, Y. Gogotsi, Y. Gao, Li-ion uptake and increase in interlayer spacing of Nb_4C_3 MXene, Energy Storage Mater. 8 (2017) 42–48.
[107] A. Byeon, A.M. Glushenkov, B. Anasori, P. Urbankowski, J. Li, B.W. Byles, B. Blake, K.L. Van Aken, S. Kota, E. Pomerantseva, J.W. Lee, Y. Chen, Y. Gogotsi, Lithium-ion capacitors with 2D Nb_2CT_x (MXene) – carbon nanotube electrodes, J. Power Sources 326 (2016) 686–694.
[108] C.E. Ren, M.-Q. Zhao, T. Makaryan, J. Halim, M. Boota, S. Kota, B. Anasori, M.W. Barsoum, Y. Gogotsi, Porous two-dimensional transition metal carbide (MXene) flakes for high-performance Li-ion storage, Chemelectrochem 3 (2016) 689–693.
[109] C.F. Zhang, B. Anasori, A. Seral-Ascaso, S.H. Park, N. McEvoy, A. Shmeliov, G.S. Duesberg, J.N. Coleman, Y. Gogotsi, V. Nicolosi, Transparent, flexible, and conductive 2D titanium carbide (MXene) films with high volumetric capacitance, Adv. Mater. 29 (2017) 1702678.
[110] A. Byeon, M.-Q. Zhao, C.E. Ren, J. Halim, S. Kota, P. Urbankowski, B. Anasori, M.W. Barsoum, Y. Gogotsi, Two-dimensional titanium carbide MXene as a cathode material for hybrid magnesium/lithium-ion batteries, ACS Appl. Mater. Interfaces 9 (2017) 4296–4300.
[111] B. Ahmed, D.H. Anjum, M.N. Hedhili, Y. Gogotsi, H.N. Alshareef, H_2O_2 assisted room temperature oxidation of Ti_2C MXene for Li-ion battery anodes, Nanoscale 8 (2016) 7580–7587.
[112] C. Zhang, S.J. Kim, M. Ghidiu, M.-Q. Zhao, M.W. Barsoum, V. Nicolosi, Y. Gogotsi, Layered orthorhombic Nb_2O_5@$Nb_4C_3T_x$ and TiO_2@$Ti_3C_2T_x$ hierarchical composites for high performance Li-ion batteries, Adv. Funct. Mater. 26 (2016) 4143–4151.
[113] B. Ahmed, D.H. Anjum, Y. Gogotsi, H.N. Alshareef, Atomic layer deposition of SnO_2 on MXene for Li-ion battery anodes, Nano Energy 34 (2017) 249–256.
[114] A.T. Tesfaye, O. Mashtalir, M. Naguib, M.W. Barsoum, Y. Gogotsi, T. Djenizian, Anodized Ti_3SiC_2 as an anode material for Li-ion microbatteries, ACS Appl. Mater. Interfaces 8 (2016) 16670–16676.
[115] M.-Q. Zhao, M. Torelli, C.E. Ren, M. Ghidiu, Z. Ling, B. Anasori, M.W. Barsoum, Y. Gogotsi, 2D titanium carbide and transition metal oxides hybrid electrodes for Li-ion storage, Nano Energy 30 (2016) 603–613.
[116] G. Zou, Z. Zhang, J. Guo, B. Liu, Q. Zhang, C. Fernandez, Q. Peng, Synthesis of MXene/Ag composites for extraordinary long cycle lifetime lithium storage at high rates, ACS Appl. Mater. Interfaces 8 (2016) 22280–22286.
[117] Q. Gao, J. Come, M. Naguib, S. Jesse, Y. Gogotsi, N. Balke, Synergetic effects of K^+ and Mg^{2+} ion intercalation on the electrochemical and actuation properties of the two-dimensional Ti_3C_2 MXene, Faraday Discuss. 199 (2017) 393–403.
[118] S. Kajiyama, L. Szabova, K. Sodeyama, H. Iinuma, R. Morita, K. Gotoh, Y. Tateyama, M. Okubo, A. Yamada, Sodium-ion intercalation mechanism in MXene nanosheets, ACS Nano 10 (2016) 3334–3341.
[119] Y. Wu, P. Nie, J. Jiang, B. Ding, H. Dou, X. Zhang, MoS_2-nanosheet-decorated 2D titanium carbide (MXene) as high-performance anodes for sodium-ion batteries, ChemElectroChem 4 (2017) 1560–1565.
[120] X. Xie, M.-Q. Zhao, B. Anasori, K. Maleski, C.E. Ren, J. Li, B.W. Byles, E. Pomerantseva, G. Wang, Y. Gogotsi, Porous heterostructured MXene/carbon nanotube composite paper with high volumetric capacity for sodium-based energy storage devices, Nano Energy 26 (2016) 513–523.
[121] S.-M. Bak, R. Qiao, W. Yang, S. Lee, X. Yu, B. Anasori, H. Lee, Y. Gogotsi, X.-Q. Yang, Na-ion intercalation and charge storage mechanism in 2D vanadium carbide, Adv. Energy Mater. (2017) 1700959.
[122] M.Q. Zhao, X.Q. Xie, C.E. Ren, T. Makaryan, B. Anasori, G.X. Wang, Y. Gogotsi, Hollow MXene spheres and 3D macroporous MXene frameworks for Na-ion storage, Adv. Mater. 29 (2017), http://dx.doi.org/10.1002/adma.201702410.
[123] P.C. Lian, Y.F. Dong, Z.S. Wu, S.H. Zheng, X.H. Wang, S. Wang, C.L. Sun, J.Q. Qin, X.Y. Shi, X.H. Bao, Alkalized Ti_3C_2 MXene nanoribbons with expanded interlayer spacing for high-capacity sodium and potassium ion batteries, Nano Energy 40 (2017) 1–8.
[124] X. Guo, X.Q. Xie, S. Choi, Y.F. Zhao, H. Liu, C.Y. Wang, S. Chang, G.X. Wang, Sb_2O_3/MXene($Ti_3C_2T_x$) hybrid anode materials with enhanced performance for sodium-ion batteries, J. Mater. Chem. A 5 (2017) 12445–12452.
[125] Y. Dall'Agnese, P.-L. Taberna, Y. Gogotsi, P. Simon, Two-dimensional vanadium carbide (MXene) as positive electrode for sodium-ion capacitors, J. Phys. Chem. Lett. 6 (2015) 2305–2309.
[126] X. Liang, A. Garsuch, L.F. Nazar, Sulfur cathodes based on conductive MXene nanosheets for high-performance lithium-sulfur batteries, Angew. Chem. Int. Ed. 54 (2015) 3907–3911.
[127] J. Song, D. Su, X. Xie, X. Guo, W. Bao, G. Shao, G. Wang, Immobilizing polysulfides with MXene-functionalized separators for stable lithium-sulfur batteries, ACS Appl. Mater. Interfaces 8 (2016) 29427–29433.
[128] H.-J. Peng, G. Zhang, X. Chen, Z.-W. Zhang, W.-T. Xu, J.-Q. Huang, Q. Zhang, Enhanced electrochemical kinetics on conductive polar mediators for lithium-sulfur batteries, Angew. Chem. Int. Ed. 55 (2016) 12990–12995.
[129] M.-Q. Zhao, M. Sedran, Z. Ling, M.R. Lukatskaya, O. Mashtalir, M. Ghidiu, B. Dyatkin, D.J. Tallman, T. Djenizian, M.W. Barsoum, Y. Gogotsi, Synthesis of carbon/sulfur nanolaminates by electrochemical extraction of titanium from Ti2SC, Angew. Chem. Int. Ed. 54 (2015) 4810–4814.
[130] B. Li, D. Zhang, Y. Liu, Y. Yu, S. Li, S. Yang, Flexible Ti_3C_2 MXene-lithium film with lamellar structure for ultrastable metallic lithium anodes, Nano Energy 39 (2017) 654–661.
[131] W.Z. Bao, X.Q. Xie, J. Xu, X. Guo, J.J. Song, W.J. Wu, D.W. Su, G.X. Wang, Confined sulfur in 3D MXene/reduced graphene oxide hybrid nanosheets for lithium-sulfur battery, Chem. Eur. J. 23 (2017) 12613–12619.
[132] D.W. Rao, L.Y. Zhang, Y.H. Wang, Z.S. Meng, X.Y. Qian, J.H. Liu, X.Q. Shen, G.J. Qiao, R.F. Lu, Mechanism on the improved performance of lithium sulfur batteries with MXene-based additives, J. Phys. Chem. C 121 (2017) 11047–11054.
[133] C. KunFeng, X. DongFeng, Rare earth and transitional metal colloidal supercapacitors, Sci. China Technol. Sci. 58 (2015) 1768.
[134] X. Chen, K. Chen, H. Wang, D. Xue, A colloidal pseudocapacitor: direct use of Fe$(NO_3)_3$ in electrode can lead to a high performance alkaline supercapacitor system, J. Colloid Interface Sci. 444 (2015) 49–57.
[135] K. Chen, D. Xue, Colloidal supercapattery: redox ions in electrode and electrolyte, Chem. Record (2017), http://dx.doi.org/10.1002/tcr.201700037.
[136] K. Chen, D. Xue, Colloidal supercapacitor electrode materials, Mater. Res. Bull. 83 (2016) 201–206.
[137] K. Chen, D. Xue, S. Komarneni, Colloidal pseudocapacitor: nanoscale aggregation of Mn colloids from $MnCl_2$ under alkaline condition, J. Power Sources 279 (2015) 365–371.
[138] K. Chen, D. Xue, High energy density hybrid supercapacitor: in-situ functionalization of vanadium-based colloidal cathode, ACS Appl. Mater. Interfaces 8 (2016) 29522–29528.
[139] M. Hu, T. Hu, R. Cheng, J. Yang, C. Cui, C. Zhang, X. Wang, MXene-coated silk-derived carbon cloth toward flexible electrode for supercapacitor application, J. Energy Chem. (2017), http://dx.doi.org/10.1016/j.jechem.2017.1010.1030.
[140] X. Ji, K. Xu, C. Chen, B. Zhang, Y. Ruan, J. Liu, L. Miao, J. Jiang, Probing the electrochemical capacitance of MXene nanosheets for high-performance pseudocapacitors, PCCP 18 (2016) 4460–4467.
[141] J. Come, Y. Xie, M. Naguib, S. Jesse, S.V. Kalinin, Y. Gogotsi, P.R.C. Kent, N. Balke, Nanoscale elastic changes in 2D Ti_3C_2Tx (MXene) pseudocapacitive electrodes, Adv. Energy Mater. 6 (2016) 1502290.
[142] Y.Y. Peng, B. Akuzum, N. Kurra, M.Q. Zhao, M. Alhabe, B. Anasori, E.C. Kumbur, H.N. Alshareef, M.D. Ger, Y. Gogotsi, All-MXene (2D titanium carbide) solid-state microsupercapacitors for on-chip energy storage, Energy Environ. Sci. 9 (2016) 2847–2854.
[143] N. Kurra, B. Ahmed, Y. Gogotsi, H.N. Alshareef, MXene-on-paper coplanar microsupercapacitors, Adv. Energy Mater. 6 (2016) 1601372.
[144] J. Li, X.T. Yuan, C. Lin, Y.Q. Yang, L. Xu, X. Du, J.L. Xie, J.H. Lin, J.L. Sun, Achieving high pseudocapacitance of 2D titanium carbide (MXene) by cation intercalation and surface modification, Adv. Energy Mater. 7 (2017) 1602725.
[145] H.B. Wang, J.F. Zhang, Y.P. Wu, H.J. Huang, Q.G. Jiang, Achieving high-rate capacitance of multi-layer titanium carbide (MXene) by liquid-phase exfoliation through Li-intercalation, Electrochem. Commun. 81 (2017) 48–51.
[146] S.K. Xu, G.D. Wei, J.Z. Li, Y. Ji, N. Klyui, V. Izotov, W. Han, Binder-free $Ti_3C_2T_x$ MXene electrode film for supercapacitor produced by electrophoretic deposition method, Chem. Eng. J. 317 (2017) 1026–1036.
[147] M.R. Lukatskaya, S. Kota, Z. Lin, M.-Q. Zhao, N. Shpigel, M.D. Levi, J. Halim, P.-L. Taberna, M.W. Barsoum, P. Simon, Y. Gogotsi, Ultra-high-rate pseudocapacitive energy storage in two-dimensional transition metal carbides, Nat. Energy 2 (2017) 17105.
[148] C. Yang, W. Que, X. Yin, Y. Tian, Y. Yang, M. Que, Improved capacitance of nitrogen-doped delaminated two-dimensional titanium carbide by urea-assisted synthesis, Electrochim. Acta 225 (2017) 416–424.
[149] C. Yang, W. Que, Y. Tang, Y. Tian, X. Yin, Nitrogen and sulfur co-doped 2D titanium carbides for enhanced electrochemical performance, J. Electrochem. Soc. 164 (2017) A1939–A1945.
[150] Z. Lin, P. Rozier, B. Duployer, P.-L. Taberna, B. Anasori, Y. Gogotsi, P. Simon, Electrochemical and in-situ X-ray diffraction studies of $Ti_3C_2T_x$ MXene in ionic liquid electrolyte, Electrochem. Commun. 72 (2016) 50–53.
[151] Z. Lin, D. Barbara, P.-L. Taberna, K.L. Van Aken, B. Anasori, Y. Gogotsi, P. Simon, Capacitance of $Ti_3C_2T_x$ MXene in ionic liquid electrolyte, J. Power Sources 326 (2016) 575–579.
[152] M. Zhu, Y. Huang, Q. Deng, J. Zhou, Z. Pei, Q. Xue, Y. Huang, Z. Wang, H. Li, Q. Huang, C. Zhi, Highly flexible, freestanding supercapacitor electrode with enhanced performance obtained by hybridizing polypyrrole chains with MXene, Adv. Energy Mater. 6 (2016) 1600969.
[153] S. Xu, G. Wei, J. Li, W. Han, Y. Gogotsi, Flexible MXene-graphene electrodes with high volumetric capacitance for integrated co-cathode energy conversion/storage devices, J. Mater. Chem. A 5 (2017) 17442–17451.
[154] E.A. Mayerberger, O. Urbanek, R.M. McDaniel, R.M. Street, M.W. Barsoum, C.L. Schauer, Preparation and characterization of polymer-$Ti_3C_2T_x$ (MXene) composite nanofibers produced via electrospinning, J. Appl. Polym. Sci. 134 (2017) 45295.
[155] M. Boota, B. Anasori, C. Voigt, M.-Q. Zhao, M.W. Barsoum, Y. Gogotsi, Pseudocapacitive electrodes produced by oxidant-free polymerization of pyrrole between the layers of 2D titanium carbide (MXene), Adv. Mater. 28 (2016) 1517–1522.
[156] J. Zhu, Y. Tang, C. Yang, F. Wang, M. Cao, Composites of TiO_2 nanoparticles deposited on Ti_3C_2 MXene nanosheets with enhanced electrochemical performance, J. Electrochem. Soc. 163 (2016) A785–A791.
[157] R.B. Rakhi, B. Ahmed, D. Anjum, H.N. Alshareef, Direct chemical synthesis of MnO_2 nanowhiskers on transition metal carbide surfaces for supercapacitor applications, ACS Appl. Mater. Interfaces 8 (2016) 18806–18814.

[158] Y. Tian, C. Yang, W. Que, X. Liu, X. Yin, L.B. Kong, Flexible and free-standing 2D titanium carbide film decorated with manganese oxide nanoparticles as a high volumetric capacity electrode for supercapacitor, J. Power Sources 359 (2017) 332–339.
[159] C. Zhang, M. Beidaghi, M. Naguib, M.R. Lukatskaya, M.-Q. Zhao, B. Dyatkin, K.M. Cook, S.J. Kim, B. Eng, X. Xiao, D. Long, W. Qiao, B. Dunn, Y. Gogotsi, Synthesis and charge storage properties of hierarchical niobium pentoxide/carbon/niobium carbide (MXene) hybrid materials, Chem. Mater. 28 (2016) 3937–3943.
[160] J. Luo, W. Zhang, H. Yuan, C. Jin, L. Zhang, H. Huang, C. Liang, Y. Xia, J. Zhang, Y. Gan, X. Tao, Pillared structure design of MXene with ultralarge interlayer spacing for high-performance lithium-ion capacitors, ACS Nano 11 (2017) 2459–2469.
[161] S. Kajiyama, L. Szabova, H. Iinuma, A. Sugahara, K. Gotoh, K. Sodeyama, Y. Tateyama, M. Okubo, A. Yamada, Enhanced Li-ion accessibility in MXene titanium carbide by steric chloride termination, Adv. Energy Mater. 7 (2017) 1601873.
[162] X. Wang, S. Kajiyama, H. Iinuma, E. Hosono, S. Oro, I. Moriguchi, M. Okubo, A. Yamada, Pseudocapacitance of MXene nanosheets for high-power sodium-ion hybrid capacitors, Nat. Commun. 6 (2015) 6544.
[163] J.O.M. Bockris, The hydrogen economy, in: J.O.M. Bockris (Ed.), Environmental Chemistry, Springer, US, Boston, MA, 1977, pp. 549–582.
[164] S.L. Candelaria, Y.Y. Shao, W. Zhou, X.L. Li, J. Xiao, J.G. Zhang, Y. Wang, J. Liu, J.H. Li, G.Z. Cao, Nanostructured carbon for energy storage and conversion, Nano Energy 1 (2012) 195–220.
[165] M. Pumera, Graphene-based nanomaterials for energy storage, Energy Environ. Sci. 4 (2011) 668–674.
[166] Q. Zhao, W. Yuan, J. Liang, J. Li, Synthesis and hydrogen storage studies of metal–organic framework UiO-66, Int. J. Hydrogen Energy 38 (2013) 13104–13109.
[167] E. Tylianakis, E. Klontzas, G.E. Froudakis, Multi-scale theoretical investigation of hydrogen storage in covalent organic frameworks, Nanoscale 3 (2011) 856–869.
[168] Q.K. Hu, D.D. Sun, Q.H. Wu, H.Y. Wang, L.B. Wang, B.Z. Liu, A.G. Zhou, J.L. He, MXene: a new family of promising hydrogen storage medium, J. Phys. Chem. A 117 (2013) 14253–14260.
[169] Q.K. Hu, H.Y. Wang, Q.H. Wu, X.T. Ye, A.G. Zhou, D.D. Sun, L.B. Wang, B.Z. Liu, J.L. He, Two-dimensional Sc_2C: a reversible and high-capacity hydrogen storage material predicted by first-principles calculations, Int. J. Hydrogen Energy 39 (2014) 10606–10612.
[170] A. Yadav, A. Dashora, N. Patel, A. Miotello, M. Press, D.C. Kothari, Study of 2D MXene Cr_2C material for hydrogen storage using density functional theory, Appl. Surf. Sci. 389 (2016) 88–95.
[171] R.Y. Wu, H.F. Du, Z.Y. Wang, M.X. Gao, H.G. Pan, Y.F. Liu, Remarkably improved hydrogen storage properties of $NaAlH_4$ doped with 2D titanium carbide, J. Power Sources 327 (2016) 519–525.